arXiv:hep-lat/9703005v1 8 Mar 1997

Hubbard Model with Lüscher fermions [1]

Paweł Sawicki [2]

Institute of Physics, Jagiellonian University,
ul. Reymonta 4, PL-30-059, Kraków

Abstract

We study the basic features of the two-dimensional quantum Hubbard Model at half-filling by means of the Lüscher algorithm and the algorithm based on direct update of the determinant of the fermionic matrix. We implement the Lüscher idea employing the transfer matrix formalism which allows to formulate the problem on the lattice in (2+1) dimensions. We discuss the numerical complexity of the Lüscher technique, systematic errors introduced by polynomial approximation and introduce some improvements which reduce long autocorrelations. In particular we show that preconditioning of the fermionic matrix speeds up the algorithm and extends the available range of parameters. We investigate the magnetic and the one-particle properties of the Hubbard Model at half-filling and show that they are in qualitative agreement with the existing Monte Carlo data and the mean-field predictions.

TPJU–4/97
March 1997

[1]Work supported in part by the KBN grants: no. 2P03B19609 and no. 2P03B04412
[2]A fellow of the Foundation for Polish Science

Contents

1 Introduction **3**

2 The Hubbard Model **4**

3 Path integral formulation of the Hubbard Model **7**

4 Algorithms **10**

4.1 Introduction 10

4.2 Algorithms based on evolution equations 11

4.3 Algorithms for simulation of the Hubbard Model 15

4.4 Local bosonic algorithm 17

4.5 Exact algorithm 19

5 Results **20**

5.1 Implementation details and the errors of the polynomial approximation 20

5.2 Dynamical properties of the Lüscher algorithm and its modifications 21

5.3 Magnetic properties of the Hubbard Model 25

5.4 Fermi surface 27

5.5 Effective hopping 28

6 Summary and conclusions **29**

A Appendix A **31**

B Appendix B **32**

1 Introduction

It is very well known that quark degrees of freedom are difficult to include in numerical simulations of quantum systems [1]. Although the substantial progress has been made in this field the search for new algorithmic techniques is an active research area. At present probably the best method is to integrate the quark degrees of freedom and simulate the theory with effective action. However such action usually contains determinant which is a nonlocal object and its evaluation is very expensive in computer time. Recently a new computational scheme has been proposed by Lüscher who showed, in the QCD case, how to approximate determinant of the Dirac operator by a local bosonic action [2]. So far there is no complete discussion of properties of this algorithm and it is of great interest to perform some tests of its performance.

Besides QCD there is a wide class of physically interesting problems where effective technique for simulating fermionic degrees of freedom is of crucial importance. The Hubbard Model [3] is an example of a conceptually simple model with effective Coulomb repulsion between electrons which for many years has been the basic framework for studying strongly correlated electrons in solid state physics. The interest of the Hubbard Model has been renewed after finding that it can qualitatively describe the magnetic properties of the high T_c superconducting materials above the temperature of the superconducting transition [4]. There is also a conjecture suggested by a variety of calculations that when two dimensional system is doped slightly away from half-filling the repulsion between electrons can give rise to superconductivity [5]. Until now this hypothesis has not been confirmed or rejected. The Hubbard Model is very well suited to tests of the new fermionic algorithms because it contains all details of fermionic formulation and describes very interesting, and rather unexplored from numerical point of view, physics of strongly correlated electrons.

In this paper we apply the Lüscher idea to the Hubbard Model. We show how to study basic features of strongly correlated electrons and note about the problems which can be solved by numerical simulations. We study the efficiency of the Lüscher algorithm in comparison with the algorithm based on direct update of the determinant of the fermionic matrix. We propose also some improvements which reduce long autocorrelation times. Some conclusions from this dicussion can be applied in implementation of the Lüscher algorithm in other areas.

The paper is organized as follows. Section 2 is assigned to the review of the basic properties of the Hubbard Model. We emphasize some important not fully solved problems. Section 3 covers path integral formulation of the Hubbard Model. In section 4 we review fermion Quantum Monte Carlo methods and introduce two new algorithms. One is the implementation of the Lüscher method to the Hubbard Model. The second is a modification of the algorithm based on direct update of the determinant of the fermionic matrix. In section 5 we compare dynamical properties of these two algorithms and present some physical results obtained from simulations of half-filled band Hubbard Model. The comparison of these results with previous

findings and theoretical predictions gives credence to our methods of simulations. Section 6 contains a summary and our conclusions.

2 The Hubbard Model

The Hubbard Model is defined by the Hubbard Hamiltonian

$$\mathcal{H} = -K \sum_{\langle i,j\rangle,\sigma} a^{\dagger}_{i\sigma} a_{j\sigma} + U \sum_{i} \left(n_{i\uparrow} - \frac{1}{2}\right)\left(n_{i\downarrow} - \frac{1}{2}\right) - \mu \sum_{i\sigma} n_{i\sigma}, \tag{1}$$

where $a_{i\sigma}$ is the annihilation operator of an electron with spin σ located at site i of d dimensional lattice. In this paper however we will concentrate mainly on the case $d = 2$, which is physically the most interesting. The summation in the kinetic term runs over nearest neighbors (each symmetric pair of $\langle i, j\rangle$ is counted twice) and the hopping energy K can be taken as a unit of energy. The interaction term takes into account short-range effective Coulomb repulsion. The term with the chemical potential determines the band filling. The half–filled band has $\mu = 0$. There are three dimensionless parameters which determine the behaviour of the system, interaction energy U/K, band filling μ/K and temperature T/K. In this parameter space the Hubbard Model exhibits various phases.

Originally the Hubbard Model was introduced as the simplest system which might exhibit an insulating (Mott) state. It is exactly soluble only in one dimension. In this case the integral equation for the density of states can be solved in a closed form [6]. It follows that the system is insulating for any nonzero U and conducting for $U = 0$. Thus there is no Mott transition at finite U. However even for 1d system we have only partial information. For example, the correlation functions are not known. In 2 and higher dimensions many different approximate techniques have been used. Mean field approximation [7], variational techniques [8] and other were successful in describing the properties of strongly correlated electrons. They are very important because they give insight into physics. Unfortunately it is very difficult to judge the accuracy of approximate techniques beyond the perturbative limit. Therefore it is not surprising that they often give conflicting results. Numerical simulations can fill this gap and deliver nonperturbative results for comparison.

Some properties of the Hubbard Model on square lattice may be understood from simple qualitative considerations. Let us start from the noninteracting limit. The dispersion relation

$$\epsilon_k = -2K(\cos k_x + \cos k_y), \tag{2}$$

establishes the band structure. The total bandwidth $E_b = 8K$. The ground state is obtained by populating the states from the bottom of the energy scale up to the Fermi level. In the half-filled case the rectangular shape of the Fermi surface is determined from the condition $\epsilon_F = 0$ as shown in Fig. 1 .

The existence of parallel sectors on the Fermi surface which are separated by the vector $Q_{nest} = (\pm\pi, \pi)$ (nesting) has important physical consequences and is crucial for the developing of the magnetic instabilities. Indeed the weak interaction

could induce the process of exchanging electrons with opposite spins from opposite sides of the Fermi surface. It involves however the exchange of momentum Q_{nest} which is characteristic for antiferromagnetism. Obviously without detailed theory it is impossible to make final conclusions. For example, there is also a process of quasi-forward scattering with the exchange of momentum $(0,0)$ which would give rise to ferromagnetism and from simple qualitative arguments it is impossible to judge which is dominant.

On the other hand, in the strong coupling limit ($U \to \infty$) the interaction term forces electrons not to reside on the doubly occupied site. The hopping term can be treated as a perturbation and the ordinary expansion in the parameter K/U is applicable. The effective Hamiltonian is the Quantum Heisenberg Antiferromagnet

$$\mathcal{H}_0 = \frac{2K^2}{U} \sum_{\langle i,j \rangle} \vec{S}_i \vec{S}_j, \tag{3}$$

with the exchange coupling $2K^2/U$. The above result is valid for the half-filled system in any dimension and lattice.

Therefore it is plausible that the Hubbard Model may possess ground state with nontrivial magnetic properties. More quantitative description can be obtained by the mean field theory. One assumes that the ground state has some sort of magnetic order and the problem can be solved by means of variational principle. Detailed calculations for the antiferromagnetic ground state is given in the Appendix A. Here we stress main results. One possible solution is the *ferromagnetic* state which can exists for sufficiently large U. The critical value is given by Stoner's criterion

$$U_{crit} \rho(\epsilon_F) > 1 \tag{4}$$

with $\rho(\epsilon_F) = \sum_k \delta(\epsilon_F - \epsilon_k)$ being the density of states on the Fermi surface. But there is also an *antiferromagnetic* solution for any U with the smaller energy which is a better candidate for the true ground state of the half-filled Hubbard Model. Numerical simulations fully confirm that expectation and the antiferromagnetic order has been explicitly proven for $U \leq 2$ [9]. It is also believed that antiferromagnetism exists for any nonzero U. Mean field solution gives also new band structure $E_k = \pm\sqrt{\epsilon_k^2 + \Delta^2}$ with the gap 2Δ above the Fermi surface characteristic for an insulator.

A lot of single-particle properties can be obtained from the study of the one particle Green's function defined by

$$G_{\sigma\sigma'}(r,t;r',t') = -i\langle T a_\sigma(r,t) a^\dagger_{\sigma'}(r',t') \rangle \tag{5}$$

where $a_\sigma(r,t)$ are annihilation operators in Heisenberg picture. T orders product of operators at earlier time to the right of operators at later time, keeping track of the sign changes associated with Fermi statistic; i. e. for two fermionic operators $A(t)$ and $B(t)$ we have

$$TA(t)B(t') = A(t)B(t')\theta(t-t') - B(t')A(t)\theta(t'-t). \tag{6}$$

For the noninteracting system, which is translationally invariant and time independent the Fourier transform of $G(r,t;r',t')$ is a function of 2 variables [10]

$$G^0_{\sigma\sigma'}(k,\omega) = \delta_{\sigma\sigma'} \lim_{\nu\to 0+} \left(\frac{\theta(\epsilon_k - \epsilon_F)}{\omega - \epsilon_k + i\nu} + \frac{\theta(\epsilon_F - \epsilon_k)}{\omega - \epsilon_k - i\nu} \right). \tag{7}$$

The poles of the propagator exhibit typical one particle spectrum. In the weakly interacting case we can expect that physical low-energy excitations look like weakly interacting fermions. The propagator retains its pole structure with a renormalized dispersion relation $\epsilon_{ren}(k)$. Thus it is expected that the propagator near the Fermi surface should look like

$$\lim_{\omega\to\epsilon_F} G(k,\omega) = \lim_{\nu\to 0+} \left(\frac{Z}{\omega - \epsilon_{ren}(k) + i\nu} + G_{reg} \right) \tag{8}$$

with a certain regular part G_{reg}. The *wave function renormalization* Z measures the discontinuity of the occupation number $n_{k\sigma} = iG_{\sigma\sigma}(k, t = 0^-)$ at the Fermi surface. The system which exhibits such behavior is called a *Fermi liquid*.

The ground state of the half-filled Hubbard Model has long range antiferromagnetic order being the result of strong interactions. Thus we may expect quite different behaviour than the mentioned above. In fact the renormalization constant Z vanish and simulations fully confirm the lack of sharp Fermi surface [11] [12].

What happens after doping still remains unclear. The approximate analytic methods are not conclusive and one has to rely on numerical calculations. Unfortunately in this case the fermionic determinants are not positive definite. As will be discussed in Section 4 this difficulty called the sign problem significantly restricts the range of predictions. Nevertheless quantum MC can still deliver useful informations. For example, it was confirmed that antiferromagnetic order is destroyed even for small doping [11] [12]. At the same time however it is not certain weather the ground state becomes the Fermi liquid. The simulations performed at the quarter filling strongly suggest the existence of the sharp Fermi surface. The situation is unclear at small doping where the sign problem is very severe. Recent simulations [13] suggest the vanishing Z as the size of lattice increases at $U = 4$. However in the last calculations the small magnetic field was introduced to alleviate the sign problem and it is not clear how it can influence results. Thus more work should be done to clarify this issues. Should the non Fermi liquid behaviour be confirmed the holes would not propagate as free entities. One possible scenario is binding of holes and possible existence of superconducting phase.

The problem of the existence of the superconducting state has been studied directly in numerical simulations [11] [12]. The appropriate observable is the correlation function for pairs

$$P(r) = \langle \Delta_i^\dagger \Delta_{i+r} \rangle. \tag{9}$$

The annihilation operator for pair is defined as

$$\Delta_i = a_{i\uparrow}(a_{i+\hat{x}\downarrow} + a_{i-\hat{x}\downarrow} \pm a_{i+\hat{y}\downarrow} \pm a_{i+\hat{y}\downarrow}) \tag{10}$$

where the (+) sign correspond to extended $s^\star$ wave, and the (−) sign to $d_{x^2-y^2}$ wave, as can be seen from rotational symmetry [14]. In the superconducting state these correlations should diverge with the spatial lattice volume. A widely used quantity to monitor such behaviour is the susceptibility

$$\chi = \sum_r P(r). \tag{11}$$

Current simulations indicate only very weak dependence of the pair correlations on lattice size what does not confirm the existence of the superconducting phase. One may argue however that the lattice sizes available for computation are too small while comparing with the correlation length for the pair.

The Hubbard Model can be modified in many ways. Adding the next-nearest neighbour hopping has very important consequences because the Fermi surface ceases to be nested. In this case critical value of U exists for the appearance of ferromagnetism. There is also some evidence that such model would be more relevant to the problem of high T_c superconductivity and recent numerical results indicate enhancement of correlation functions for pairs [15]. These issues are still intensively studied.

Contrary to the results discussed above the superconducting phase has been found for the attractive Hubbard Model i.e. with the reversed sign in front of U [16]. In this case the QMC simulations are much simpler since the sign problem does not occur. It might appear that physics of the attractive and the repulsive model should be very similar because both models are related by a change of sign in U and the exchange of chemical potential and magnetic field. However there is no evidence that the attractive model can serve us as an effective model for some range of parameters of the repulsive model, where one would expect pairing. Thus, at present simulations of the attractive model simply are not a solution of the sign problem.

3 Path integral formulation of the Hubbard Model

In this section we derive the path integral formulation of the Hubbard Model. Decoupling of interaction terms by means of the Hubbard-Stratonovich transformation and applying transfer matrix formalism allows to write the expression for the partition function in such a form that it can be used as a starting point for Lüscher local bosonic approximation.

Our derivation of the Euclidean path integral partition function follows closely that presented by Creutz [17]. All arguments apply essentially for both: the attractive and the repulsive Hubbard Model. However there are also some important differences which will be stressed. We begin with the Hamiltonian Eq. (1), which may be rewritten as

$$\mathcal{H} = -K \sum_{\langle i,j\rangle\sigma} a^\dagger_{i\sigma} a_{j\sigma} - \frac{U}{2} \sum_i (n_{i\uparrow} - n_{i\downarrow})^2 - \mu \sum_{i\sigma} n_{i\sigma}. \tag{12}$$

We assume that i and j are sites on a two dimensional square lattice with $N = N_x^2$ sites. This formula differs from the standard one for the repulsive Hubbard Model by an irrelevant additive constant.

All thermodynamic functions for a many particle system in the temperature T can be obtained from the partition function

$$Z = Tr[\exp -(\mathcal{H}/T)]. \tag{13}$$

Tr denotes the sum over the complete set of physical states. The thermal expectation value of some physical observable, say $\mathcal{O}$, is defined by

$$\langle \mathcal{O} \rangle = Tr[\mathcal{O} \exp -(\mathcal{H}/T)]/Z. \tag{14}$$

Unfortunately, it is usually very difficult to evaluate the trace in Eq. (14) exactly for physically interesting systems. Lattice field theory offers an interesting possibility to evaluate the expectation values for finite systems employing stochastic methods.

In the lattice formulation one interprets the inverse temperature, $1/T$, (which is also referred to as Euclidean time) as the extra dimension and discretizes it dividing the interval $(0, \beta = 1/T)$ into N_t slices of length $\epsilon = \beta/N_t$. The partition function can be written as

$$Z = Tr[(e^{-\beta\mathcal{H}/N_t})^{N_t}]. \tag{15}$$

In the next step the separation between kinetic $\mathcal{K}$ and interaction $\mathcal{V}$ term is performed according to the Trotter formula

$$e^{\epsilon\mathcal{H}} = e^{\epsilon\mathcal{K}} e^{\epsilon\mathcal{V}} + O(\epsilon^2), \tag{16}$$

which starts the series of approximations in which the terms of order of $O((\beta/N_t)^2)$ are consistently neglected

$$\begin{aligned} e^{-\beta\mathcal{H}/N_t} &= \exp\left[\frac{K\beta}{N_t} \sum_{\langle i,j\rangle\sigma} a^\dagger_{i\sigma} a_{i\sigma}\right] \\ &\quad \exp\left[\frac{U\beta}{2N_t} \sum_i \left(a^\dagger_{i\uparrow} a_{i\uparrow} - a^\dagger_{i\downarrow} a_{i\downarrow}\right)^2 + \frac{\mu\beta}{N_t} \sum_{i,\sigma} a^\dagger_{i\sigma} a_{i\sigma}\right]. \end{aligned} \tag{17}$$

As all the terms presented in the last exponent commute with each other we can treat them as ordinary numbers. In particular one can use the identity

$$\int_{-\infty}^{\infty} e^{-ax^2/2+bx}\, dx = (2\pi)^{1/2} e^{b^2/2a}, \;\; a > 0\,, \tag{18}$$

which is a continuous version of the Hubbard-Stratonovich transformation. With this in mind we can introduce the integration over auxiliary set of variables A_i located on the lattice sites to decouple the quartic term

$$\begin{aligned} e^{-\beta\mathcal{H}/N_t} = (2\pi)^{-N^2/2} \int [DA_i] e^{-\sum_i A_i^2/2} \exp\left[\frac{K\beta}{N_t} \sum_{\langle i,j\rangle\sigma} a^\dagger_{i\sigma} a_{i\sigma}\right] \\ \exp\left[\sum_i (U\beta/N_t)^{1/2} A_i (a^\dagger_{i\uparrow} a_{i\uparrow} - a^\dagger_{i\downarrow} a_{i\downarrow}) + \frac{\mu\beta}{N_t} \sum_{i,\sigma} a^\dagger_{i\sigma} a_{i\sigma}\right]. \end{aligned} \tag{19}$$

Note an ambiguity which appears in the last expression, namely which sign should have square root of $(n_{i\uparrow} - n_{i\downarrow})^2$. Two possible options are equally good and we arbitrary choose one. In principle the asymmetry between up and down components should vanish after performing functional integral over A_i and should not affect the measured observables. However due to further finite N_t approximations the corresponding results for two spin components will differ in real simulations.

To clarify the positivity of the final fermionic determinant it is convenient to formally recover the symmetry between up and down polarizations by performing the particle-hole transformation. Introducing the creation operators for hole $b_i^\dagger = (-1)^{i_x+i_y} a_{i\downarrow}$ and denoting $a_{i\uparrow}$ simply by a_i we get

$$e^{-\beta\mathcal{H}/N_t} = (2\pi)^{-N^2/2} \int [DA_i] e^{-\sum A_i^2/2} \exp\left[\frac{K\beta}{N_t} \sum_{\langle i,j\rangle} (a_i^\dagger a_j + b_i^\dagger b_j)\right]$$
$$\exp\left[\sum_i (U\beta/N_t)^{1/2} A_i (a_i^\dagger a_i + b_i^\dagger b_i - 1) - \frac{\mu\beta}{N_t} \sum_i (a_i^\dagger a_i + b_i^\dagger b_i)\right], \qquad (20)$$

which is explicitly symmetric in a_i and b_i operators. The sum in the exponents can be expressed as products with help of the following relations

$$\exp(a_i^\dagger a_j) = 1 + a_i^\dagger a_j \;\; (i \neq j) \quad , \quad \exp(\alpha a_i^\dagger a_i) = 1 + a_i^\dagger a_i (e^\alpha - 1) \qquad (21)$$

After collecting time slices together and shifting the A_i integration the resulting trace of normal ordered products takes the form:

$$Z = \exp[N^2\beta(U/2) + \mu)](2\pi)^{-N^2 N_t/2}$$
$$\int [DA_{i,t}] e^{-\sum_{i,t} A_{i,t}^2/2} Tr \prod_t : \Big[\prod_{\langle i,j\rangle} [1 + (K\beta/N_t) a_i^\dagger a_j]$$
$$\prod_i (1 + a_i^\dagger a_i \{\exp[(U\beta/N_t)^{1/2} A_{i,t} - (U-\mu)\beta/N_t] - 1\})$$
$$(\{a, a^\dagger, \mu\} \to \{b, b^\dagger, -\mu\})\Big] : \qquad (22)$$

For every time slice, labeled by a discrete index $t = 1, \ldots, N_t$ the anticommutation relations can be used to convert this expression into a sum of normal ordered operators, neglecting higher orders in β/N_t . The trace can be expressed as a Grassmann integral. In Appendix B we present the general formalism of the Grassmann variables and the derivation of the partition function. The final result is

$$Z = \mathcal{N} \int [DA_{i,t}] e^{-\sum_{i,t} A_{i,t}^2/2} \det M_+ \det M_-, \qquad (23)$$

where $\mathcal{N}$ is some normalization constant. The matrices M_+ and M_- are specified by their elements between arbitrary vectors $\psi^\star$ and ψ

$$\psi^\star M_\pm \psi = \frac{K\beta}{N_t} \sum_{\langle i,j\rangle,t} \psi_{i,t}^\star \psi_{j,t} + \sum_{i,t} \psi_{i,t}^\star (\psi_{i,t} - \psi_{i,t-1})$$
$$+ \sum_{i,t} \psi_{i,t}^\star \psi_{i,t} \{\exp[(U\beta/N_t)^{1/2} A_{i,t} - (U \mp \mu)\beta/N_t] - 1\}. \qquad (24)$$

The antiperiodic boundary conditions $\psi_{i,0} = -\psi_{i,N_t}$ are taken in the t direction and reflect the Grassmann nature of the fermionic fields (see Appendix B). The M matrices are not Hermitian. It seems to be an intrinsic property of the systems with Galilean group of symmetry and can not be simply avoided [18]. This fact is rather disadvantageous for effective implementation of the Lüscher method as can be seen later.

Our expression for the partition function is rather nonstandard. We decided to work in the representation with dimension $V = NN_t$ to avoid multiplication of matrices present in the standard formulation (cf Eq. (49)). Moreover to obtain the simple structure for the matrix M we performed the series of approximations in the parameter $\epsilon = \beta/N_t$ treating the higher order terms in such a way to get the simplest possible form of matrices $M_\pm$. Due to these approximation our expression for the partition function becomes exact only as $N_t \to \infty$. In principle all measured quantities should be obtained by extrapolation to this limit.

The half-filled case is favoured from the computational point of view because then the statistical weights are positive

$$\det M_+ \det M_- = \det M^2 \tag{25}$$

since $M = M_- = M_+$. The same it is not true outside half-filling and the sign problem occurs (see Section 4). Attractive Hubbard model is more tractable as the distribution is positive definite for any μ. The interaction term can be written as

$$-\frac{|U|}{2}\sum_i (n_{i\uparrow} + n_{i\downarrow})^2. \tag{26}$$

and the derivation follows essentially the same steps. However in contrast to the previous case after performing the Hubbard-Stratonovich transformation the transfer matrix remains symmetric in the spin components and the particle hole transformation is superfluous. The statistical weights in the final result are evidently positive definite

$$Z = \mathcal{N}' \int [DA_{i,t}] e^{-\sum_{i,t} A_{i,t}^2/2} (\det M_+)^2. \tag{27}$$

The matrix M_+ is still given by Eq. (24) with U replaced by $|U|$.

4 Algorithms

4.1 Introduction

The numerical difficulties with fermionic fields come from their anticommuting nature. The transfer matrix is an operator in a Grassmann space and its matrix elements cannot be interpreted directly as a probability in Monte Carlo algorithms. For many interesting problems the formalism similar to the described above can be used to integrate the fermionic degrees of freedom. Once the final expression

for the partition function is given in closed numerical form standard techniques of stochastic sampling can be applied.

Unfortunately fermionic determinants appearing in the partition function are non–local objects. This means that local updates require calculations which depend on the state of the whole system. Thus to update the fields individually on each lattice site, or link, soon becomes prohibitively expensive in computer time as the size of system grows. At present, for example in the QCD case, the best known algorithms update many degrees of freedom simultaneously.

Additionally to the nonlocality of the action one has often another difficulty with lattice fermions known as a doubler problem. It is for example evident in the lattice formulation of QCD where the species of quarks are doubled in the simplest scheme incorporating the chiral symmetry. There are two popular approaches for dealing with this difficulty. In the Kogut-Suskind formulation each site carries only a single component of the Dirac spinor. In the Wilson formulation chiral symmetry of Lagrangian is explicitly broken and it is expected to be restored only in the continuum limit [19]. The Hubbard Model is physically defined on the lattice and hence the doubler problem does not appear in its path integral formulation.

In this section we review some fermionic algorithms. We discuss the algorithms based on evolution equations which are widely used in QCD and algorithms developed specially for simulations of the Hubbard Model. Afterwards, we present two particular algorithms which we use for simulations of the Hubbard Model. One is the application of the Lüscher idea to the path integral representation, which we discussed in the previous section. The second is a modification of the algorithm based on direct computation of the determinant and was introduced as a reference point for the comparison of results and efficiency of the Lüscher algorithm.

4.2 Algorithms based on evolution equations

To be more specific we concentrate on the action typical for fermionic problems

$$Z = \int [DA] e^{-S_B(A)} \det \mathcal{M}(A). \tag{28}$$

We denote the bosonic part of the action depending on the field A (which is the Hubbard–Stratonovich field for the Hubbard Model) by $S_B(A)$. The matrix $\mathcal{M}$ contains all details of fermionic formulation and its explicit form depends on the model. We assume that matrix $\mathcal{M}$ is positive definite. For example in simulations of the half-filled Hubbard Model $\mathcal{M} = M^\dagger M$ with matrix M given by Eq. (24).

The determinant of the matrix $\mathcal{M}$ can be expressed as a gaussian integral over a set of auxiliary complex fields ϕ

$$Z = \int [DA][d\phi][d\phi^\star] e^{-S_B + \phi^\star \mathcal{M}^{-1} \phi}. \tag{29}$$

The problem of evaluating determinant is now reduced to the of inversion of matrix $\mathcal{M}$. Each time components of the A field are changed the evaluation of new $\mathcal{M}^{-1}$

matrix is required. The problem is slightly simplified because for local actions $\mathcal{M}$ is sparse. In this case there are some useful iterative schemes appropriate for this task. Commonly used is the conjugate gradient algorithm [21].

However the inversion of the matrix still requires a lot of CPU time. Hence to reduce the computational effort many approximate algorithms have been proposed. One of the simplest and interesting is the *pseudofermion* method [20]. In this approach one considers only small changes in the A field linearizing the change of the action

$$\frac{dS}{dA} = \frac{dS_B}{dA} - Tr\left(\mathcal{M}^{-1}\frac{d\mathcal{M}}{dA}\right) \tag{30}$$

with

$$S = S_B - Tr \log \mathcal{M}(A). \tag{31}$$

For the local matrix $\mathcal{M}$ the quantity $\frac{d\mathcal{M}}{dA}$ can be easily calculated. The elements of the $\mathcal{M}^{-1}$ can be obtained as the appropriate correlation functions

$$(\mathcal{M}^{-1})_{ij} = \langle \chi_j^\star \chi_i \rangle. \tag{32}$$

The expectation value is taken over complex fields χ, called *pseudofermions* which are distributed according to the formula

$$P(\chi) \propto \exp\left(-\chi^\star \mathcal{M} \chi\right). \tag{33}$$

Fields χ can be easily simulated giving the estimation for the elements of matrix $\mathcal{M}^{-1}$. Such estimation is usually done once per full sweep of the variables A. The assumption of small changes, which can be realized by taking sufficiently small step for proposing trial values of the A field is very important. The algorithm is only approximate and in principle all measured quantities should be obtained by extrapolation with the size of the step going to zero. In practice such analysis is rarely made due to the insufficient computing resources. The algorithm described above usually has long autocorrelations and is inefficient. However it was the starting point for developing new better approaches.

Another very friutfull idea refers to stochastic equations, which can be used to generate the fields with the probability distribution (28). For sake of simplicity we restrict the discussion to a single degree of freedom. Further generalization to the field theory is straightforward. Let us consider a particle with mass m moving in a potential $V(x)$. To the Newton's equation of motion we add also a drag force proportional to the velocity and a randomizing force

$$m\frac{d^2x}{d\tau} = -\frac{dV}{dx} - \alpha\frac{dx}{d\tau} + \left(\frac{2\alpha}{\gamma}\right)^{1/2}\eta(\tau) \tag{34}$$

with α and γ being free parameters. The random force is white noise $\langle \eta(\tau)\eta(\tau') = \delta(\tau - \tau')\rangle$. Detailed definition of the distribution $\rho(\eta)$ of will be given later. The coefficient in front of η is a matter of convention. After introducing the momentum

p the equation can be rewritten as a system of two first order equations

$$\begin{aligned} \frac{dp}{d\tau} &= -\frac{dV}{dx} - \frac{\alpha p}{m} + \left(\frac{2\alpha}{\gamma}\right)^{1/2} \eta(\tau) \\ \frac{dx}{d\tau} &= \frac{p}{m}. \end{aligned} \tag{35}$$

For the simulation purposes we divide the time τ into slices of size ϵ. The quantities x' and p' at time $\tau + \epsilon$ can be calculated from x and p at time τ from the formulas

$$\begin{aligned} p' &= p + \epsilon \left[-\frac{dV}{dx} - \frac{\alpha p}{m} + \left(\frac{2\alpha}{\gamma}\right)^{1/2} \eta(\tau) \right], \\ x' &= x + \frac{\epsilon p'}{m}. \end{aligned} \tag{36}$$

To minimize the errors of discretization special form of update was introduced. The momentum p is calculated first and this new value is used to update x. In the limit of deterministic evolution this "leap-frog" scheme of integration preserves phase space volumes (the Jacobian of the transformation equals 1) and is reversible under the change of the sign of ϵ . These properties are very useful in making the algorithm exact.

The quantity η is generated, independently for each discretized slice of the evolution time, according to distribution

$$\rho(\eta) = \sqrt{\frac{\epsilon}{2\pi}} e^{-\eta^2 \epsilon/2}. \tag{37}$$

which implies that

$$\int \rho(\eta) \eta^j d\eta = \begin{cases} = 1, & j = 0 \\ = 0, & j = 1 \\ = 1/\epsilon & j = 2 \\ = O(\epsilon^{-j/2}) & j \geq 3 \end{cases} . \tag{38}$$

Let us denote a probability density of finding the state with given x and p by $P(x,p)$. Updating the states gives a new ensemble with the probability distribution

$$\begin{aligned} P'(x',p') &= \int dx\, dp\, P(x,p) P(x,p \to x',p') \\ &= \int dx\, dp\, d\eta\, \rho(\eta) P(x,p) \\ &\quad \times \delta \left(p' - p - \epsilon \left[-\frac{dV}{dx} - \frac{\alpha p}{m} + \left(\frac{2\alpha}{\gamma}\right)^{1/2} \eta(\tau) \right] \right) \\ &\quad \times \delta(x' - x - \frac{\epsilon p'}{m}). \end{aligned} \tag{39}$$

A little algebra yields the result

$$\begin{aligned} P'(x,p) &= P(x,p) \\ &+ \epsilon \left[\left(\frac{\partial H}{\partial x}\frac{\partial P}{\partial p} - \frac{\partial H}{\partial p}\frac{\partial P}{\partial x} \right) + \alpha \left(\frac{1}{\gamma}\frac{\partial^2 P}{\partial p^2} + \frac{p}{m}\frac{\partial P}{\partial p} + \frac{P}{m} \right) \right] + O(\epsilon^2), \end{aligned} \tag{40}$$

whrere H is the Hamiltonian corresponding to the original Newton's equation of motion $H = \frac{p^2}{2m} + V(x)$. Eq. (40) is a Fokker-Planck equation for the evolution of the probability distribution $P(x,p)$. It is now readily verified to order ϵ that stationary distribution for such evolution is the simple Boltzman weight

$$P(x,p) = \exp\{-\gamma H(p,x)\} \tag{41}$$

which can be obtained through the very long evolution.

In the limit $m \to 0$ the Eq. (34) leads to the Langevin equation in the rescaled time ($\tau \to \alpha\tau$)

$$\frac{dx}{d\tau} = -\frac{dV}{dx} + \left(\frac{2}{\gamma}\right)^{1/2} \eta(\tau). \tag{42}$$

In the limit $\alpha \to 0$ one recovers the deterministic limit called also microcanonical. Since in that case we get back to the Newton's equation and the energy remains unchanged during evolution the temperature should be measured by some sort of thermometer. In our example it could be the average kinetic energy of the particle $\frac{1}{2}kT = \langle\frac{p^2}{2m}\rangle$. To change the temperature one should start from different initial configuration.

Both approches: Langevin and microcanonical were used in numerical simulations of fermions [22] [23]. In the standard version Hybrid Monte Carlo (HMC) algorithm [24] makes use of deterministic evolution equations. For illustration purposes we consider the HMC algorithm for the half-filled Hubbard Model. Introducing for every A_i the corresponding momentum p_i the Hamiltonian of the system can be written as

$$H(A,p) = \frac{1}{2}\sum_i p_i^2 + \frac{1}{2}\sum_i A_i^2 + \sum_{i,j} \phi_i^\star (M^\dagger M)^{-1}_{i,j} \phi_j, \tag{43}$$

where the indices i and j run over the whole space-time lattice. Initially the gaussian momenta p are chosen and fields ϕ are generated from gaussian vectors r by $\phi = M^\dagger(A)r$. Then the system evolves for N_{mic} steps. The evolution equations are:

$$\dot{A}_i = \frac{\partial H}{\partial p_i}, \quad \dot{p}_i = -\frac{\partial H}{\partial A_i}. \tag{44}$$

The integration of Eqs. (44) is performed according to the leap-frog scheme with a discrete step ϵ, $N_{mic}\epsilon$ is the trajectory length. The conjugate gradient algorithm is required to compute the new vector $(M^\dagger M)^{-1}\phi$ in each step of the evolution.

Due to the finite step errors the energy does not remain constant during the evolution. Thus to ensure the exactness of the algorithm additional global reject/accept step is needed. According to Metropolis scheme one can fully restore the detailed balance by accepting the new configuration (p', A') with the probability

$$P_{acc} = \min[1, \exp\left(H(p,A) - H(p',A')\right)] \tag{45}$$

The acceptance rate behaves as

$$P_{acc} = erfc(cN_{mic}\epsilon^3\sqrt{V}), \tag{46}$$

where V is the total volume of the lattice and c is a constant factor. The errror function $erfc$ is defined as

$$erfc(x) = \frac{2}{\sqrt{\pi}} \int_x^\infty e^{-t^2}\, dt\ . \tag{47}$$

If the trajectory length is fixed the acceptance falls exponentially with ϵ^4. Thus to minimize the autocorrelations one should keep the step size as large a possible still maintaining reasonable acceptance.

Currently it is the most widely used algorithm in simulations with dynamical quarks in QCD. In the optimal situation its numerical complexity behaves with the volume of the system as $VV^{1/4}$, as can be readily verified from Eq. (46) which is only slightly worse than the linear dependence for bosonic algorithms. However these algorithms are still rather complicated comparing with the simplicity of pure bosonic algorithms and suffer from the strong autocorrelations between generated configurations. The proof of the detailed balance of the HMC algorithm requires exact reversibility and it is unclear how finite numerical accuracy of calculations can influence the reversibility of the algorithm and further the physical results [25]. As can be seen later Lüscher method has no such difficulties. The resulting action is local and systematic errors are under control.

4.3 Algorithms for simulation of the Hubbard Model

It is rather surprising that the algorithms described above have not been widely used for simulations of the Hubbard Model. Only recently extensive studies of the attractive Hubbard Model has been performed with the help of HMC algorithm [26]. Today's leading algorithm [11] is based rather on the exact numerical evaluation of the determinants appearing in the expression for the partition function. Assuming that the two dimensional lattice with spatial volume $N = N_x N_y$ and N_t time slices is considered, the partition function in Hirsch formulation reads [27]

$$Z = \sum_{s_{i,l}=\pm 1} \det M^+(s) \det M^-(s). \tag{48}$$

Here

$$M^\sigma = I + B^\sigma_{N_t} B^\sigma_{N_t-1} \dots B^\sigma_1 \tag{49}$$

and

$$B^\pm_l = e^{\mp \Delta\tau \nu(l)} e^{-\Delta\tau \widehat{K}} \tag{50}$$

I is the unit matrix, $\nu(l)_{i,j} = \delta_{i,j} s_{i,l}$ and $\widehat{K}$ is the matrix representation of the kinetic part of Hamiltonian. The s is the Ising like Hubbard-Stratonovich field which has two values $+1$ or -1. The index i labels the lattice sites and l the time slices. The M^σ matrices are $N \times N$ dimensional. A direct evaluation of the determinant requires $O((NN_t)^3)$ operations. Fortunately due to the very simple form of matrices there is a method of updating the determinant with $O(N^3 N_t)$ operations needed to perform full sweep through the lattice. The early implementations of this algorithm suffered from numerical instabilities especially strong in the limit of low

temperatures and extrapolation to the ground state was impossible. It turned out that numerical instabilities occurred during multiplication of the badly conditioned matrices B with almost linearly dependent columns. A simple remedy was the periodic reorthogonalization of the fermionic matrices and gave very good results. At present simulations of the half–filled Hubbard Model can deliver results with decent precision in the wide range of parameters.

An extremely difficult and not fully solved problem, referred to as the sign problem, concerns the simulation of the fermionic system when the determinant is not always positive. This is the case of the Hubbard Model outside half-filled band. A simple method for dealing with this difficulty consists of attaching the unwanted sign of the probability measure to the observable. More precisely, if P is not positively definite then the expectation value of some observable O can be written as

$$\langle O \rangle_P = \frac{\langle O sign(P) \rangle_{|P|}}{\langle sign(P) \rangle_{|P|}} \tag{51}$$

where $\langle \ldots \rangle_{|P|}$ means the expectation value with the respect to the absolute value of P. Unfortunately the above equation, exact in principle, dramatically increases statistical errors when the expectation value of sign becomes small. It is remarkable that the sign problem is especially strong just below half-filling where there is a greatest chance of finding the superconducting phase [11].

It seems that modification of the standard Quantum Monte Carlo algorithms called Projector Quantum Monte Carlo will be more useful for obtaining the ground state property of the Hubbard Model. In this approach, proposed in Ref. [28] for bosonic systems and applied further to the Hubbard Model [29], the projected partition function is introduced

$$Q = \langle \psi_T | \exp\left[-\beta \mathcal{H}\right] | \psi_T \rangle \tag{52}$$

$|\psi_T\rangle$ is a trial wave function nonorthogonal to the ground state (usually the Slater determinant). The Hamiltonian is used to systematically project the trial wave function onto the ground state. Thus in the limit of large imaginary time β the properties of the ground state can be obtained. The quantity Q can be evaluated by the Monte Carlo methods after rewriting it as a path integral.

The very interesting point is the possibility of circumventing the sign problem in this approach. It can be achieved by the appropriate choice of the trial function. It can be also handled by applying another statistical weight which gives the identical distribution in the low temperature limit with the reasonable expectation value of sign. The construction of better probabilistic weights is rather problem dependent, some simple examples are given in Ref. [29]. Recently similar philosophy has been applied to the noninteracting electron system with chemical potential [30]. The desired distribution is constructed iteratively with the help of the cluster algorithm. It was shown that for this simple model the sign problem can be completely eliminated. Of course it would be of great interest to extend this method to more complicated models.

Efficiency of the Projector Quantum Monte Carlo algorithm depends on the type of the ground state for noninteracting system (U=0). Usually if the ground

state is unique the convergence is easily achieved. Conversely in the case of the degenerate ground state the algorithm suffers from the negative sign problem and poor statistics.

According to Eq. (2) the allowed states in the momentum space can be divided into groups (shells) with a given energy. Degeneracy in the ground state appear as a result of the existence of not completely occupied shell. More precisely, if m electrons with the specified polarization occupy the shell which can contain maximally up to n such electrons it leads to a degeneracy

$$N_d = \left(\begin{array}{c} n \\ m \end{array} \right). \tag{53}$$

Although there is no analytical expression which gives the degeneracy as a function of lattice size and total number of electrons it is easy to compute this degeneracy numerically dividing the states in the momentum space into shells. As an example we consider a system with almost half-filled band, 7 electrons up and 7 electrons down on the 4×4 lattice. The ground state has a degeneracy of $N_d = 29$, as far as the sub-space of total momentum $Q = 0$ is considered. Therefore we may expect rather poor efficiency of PQMC algorithm in this physically important case.

Quite different numerical approach is based on the exact diagonalization of many particle Hamiltonian. The main problem is the enormous dimension of the Fock space $D_{Fock} = 4^N$. Fortunately symmetries of the problem often significantly reduce this number. Although the dimension of matrices precludes their direct diagonalization it is relatively easy to obtain eigenvectors for few largest and smallest eigenvalues using Lanczos method [31]. They contain all necessary information needed to compute physical observables. Additional very nice feature of this method is the ability to obtain the interesting quantities directly in the Minkowski time (real frequency properties). In Quantum Monte Carlo calculations are carried out in imaginary time and the statistical errors inherent to the Monte Carlo make the analytical continuation difficult.

4.4 Local bosonic algorithm

Recent proposal of Lüscher has attracted a lot of interest [2]. Originally being introduced as an alternative to the Hybrid Monte Carlo algorithms in QCD, soon has been applied in QMC simulations of the Hubbard Model [32]. The basic idea of Lüscher consists in approximating of the inverse of the fermionic matrix with a polynomial P_n of even degree. Its particular form being proposed is built from Chebyshev polynomials and gives rapid uniform convergence to the function $1/x$ in the interval $(\epsilon, 1)$, with ϵ being a small positive number

$$\lim_{n\to\infty} P_n(x) = 1/x. \tag{54}$$

The relative error of the approximation defined as $R_n(x) = xP_n(x) - 1$ is exponentially bounded

$$|R_n(x)| < 2\left(\frac{1-\sqrt{\epsilon}}{1+\sqrt{\epsilon}}\right)^{n+1}. \tag{55}$$

Approximation region should cover the whole spectrum of the fermionic matrix or at least its significant part. Therefore it is impossible to apply directly the original Lüscher polynomial P_n to the nonhermitian matrix M with eigenvalues distributed on the complex plane. Instead, we wrote the polynomial approximation for the matrix $Q^\dagger Q = M^\dagger M/\lambda_{max}$, where λ_{max} is the largest eigenvalue of $M^\dagger M$. Hermitian and positive definite matrix $Q^\dagger Q$ has properly distributed eigenvalues in the interval $(0, 1)$.

$$\begin{aligned}\frac{1}{Q^\dagger Q} = P_{2n}(Q^\dagger Q) = \prod_{k=1}^{2n}(Q^\dagger Q - z_k) \\ = \prod_{k=1}^{n}(Q^\dagger Q - \alpha_k - i\beta_k)(Q^\dagger Q - \alpha_k + i\beta_k)\end{aligned} \tag{56}$$

since the roots $z_k = \alpha_k + i\beta_k$ of real polynomial P_{2n} come in complex conjugate pairs. Their values are analytically known with the accuracy of $O(1/n)$. More precise values can be simply obtained by applying few Newton-Raphson iterations. After introducing auxiliary fields ϕ_k the local bosonic representation for the partition function of the Hubbard Model reads

$$Z \simeq \int [dAd\phi] e^{-S}, \tag{57}$$

where

$$S = \sum_i A_i^2/2 + \sum_{i,j}\sum_{k=1}^{n} \phi^\star_{k,i}\left[(Q^\dagger Q - \alpha_k)^2 + \beta_k^2\right]_{ij}\phi_{k,j} \tag{58}$$

with M given by Eq. (24).Here the indices i and j run over the whole space-time lattice with volume $V = N_x^2 \times N_t$. The action can be rewritten also directly in terms of the real and the imaginary part of $\phi_{k,i} = \phi^{(0)}_{k,i} + i\phi^{(1)}_{k,i}$

$$S = \sum_i A_i^2/2 + \sum_{i,j}\sum_{r=0,1}\sum_{k=1}^{n} \phi^{(r)}_{k,i}\left[(Q^\dagger Q - \alpha_k)^2 + \beta_k^2\right]_{ij}\phi^{(r)}_{k,j}. \tag{59}$$

Some remarks are in order. The resulting action S contains only local interactions. Hence we can study the fermionic system using bosonic Monte Carlo techniques. However some complications are introduced by the presence of next-to-nearest neighbors interactions. The condition number of matrix $Q^\dagger Q$ is square of condition number for M and we may generally expect the poorer behaviour of numerical procedures. Moreover it complicates the implementation of this algorithm on vector and parallel computers. The analogical action for QCD is simpler because one make use of additional symmetry of the Dirac operator.

To define the normalized matrix Q we used the upper bound for the λ_{max} which can be easily derived

$$\lambda_{max} < 2[\lambda_{max}(A^\dagger A) + \max(D)^2] \tag{60}$$

where D is diagonal part of $M = A + D$. Large magnitudes of the A fields are naturally cut by the gaussian part of the action and we may safely assume maximal value for the diagonal elements; e. g. the $A(x) < 4$ would correspond to four standard deviations assuming that the gaussian part of the action dominates.

4.5 Exact algorithm

Below we discribe algorithm based on direct computation of fermionic determinant. We use this algorithm as a kind of reference point which, first allows us by comparison to control the accuracy of the Lüscher algorithm, and second gives us a chance to compare an efficiency.

The idea of exact algorithm is based on the updating scheme allowing to compute changes in M^{-1} matrix while making trial changes in matrix M. In order to update the field A_k located on the site k one must calculate the ratio of the fermion determinants. Since the only A dependent elements of matrix M lie on the diagonal we consider the following change in the matrix M

$$M' = M + \Delta, \tag{61}$$

where Δ is matrix with one nonzero element, say k-th on the diagonal, $\Delta_{ij} = \delta_{ik}\delta_{kj}d$. Then

$$\frac{\det M'}{\det M} = \det\left(I + M^{-1}\Delta\right) = 1 + M^{-1}_{kk}d \tag{62}$$

is determined completely by elements of matrix M^{-1}. Once the trial change has been accepted the updated M^{-1} can be evaluated from the Shermann-Morrison formula [33]

$$M'^{-1} = M^{-1} - \frac{M^{-1}\Delta M^{-1}}{1 + dM^{-1}_{kk}}. \tag{63}$$

This process is economical from the computational point of view since one update of M^{-1} requires $O(V^2)$ operations comparing with $O(V^3)$ operations needed to evaluate the determinant with the brute force method. Today's leading QMC simulations of the Hubbard Model are essentially based on it [11]. As has been previously reported numerical instabilities often appear in such calculations especially at low temperatures. However our particular formulation of path integrals does not require multiplication of badly conditioned matrices and we believe that it is free of this difficulty. Indeed we performed thousands sweeps at β as large as 8 without accumulating numerical errors. However the additional cost comes from working with larger matrices.

5 Results

In this section we present implementation details of the Lüscher algorithm. We compare the accuracy and efficiency of the local bosonic algorithm with the exact algorithm described in the previous section. We use these algorithms to study basic features of the Hubbard Model. In our studies we looked mainly at the magnetic properties of the Hubbard Model and one-particle Green's functions (shape of the Fermi surface and effective hopping). Due to the sign problem our discussion is restricted to the half-filled band.

5.1 Implementation details and the errors of the polynomial approximation

The goal of the MC simulation is to generate A and ϕ fields with the disribution (57). To achieve this goal we alternately update all components of A and all components of ϕ. We first consider the update of ϕ fields. Because of the gaussian form of ϕ dependent part of the action in Eq. (57) we applied the heat bath algorithm [34] to update this sector. This is implemented as follows. For every $\phi^{(r)}_{k,i}$ component we compute the conditional parameters of its gaussian distribution while keeping other components fixed. Then the value obtained from gaussian random number generator is assigned to the $\phi^{(r)}_{k,i}$. In a full sweep through the lattice these operations are performed for each i, r and k.

The effective action depends on A in more complicated way and and the heat–bath algorithm is not longer useful. Instead we use a more general Metropolis algorithm [35]. The trial part of a single update relies on proposing a change

$$A_i = A_i + a(x - 0.5). \tag{64}$$

The Metropolis step accepts the proposed change with the probability $\min(e^{-\Delta S}, 1)$, where ΔS is corresponding change of the action. This guarantees the detailed balance condition. x is a random number uniformly distributed in the interval $(0, 1)$. The parameter a introduces the scale of changes and it is very important to tune it to get minimal autocorrelation times. Usually it is choosen to keep the acceptance ratio near 50% . It is also very important to maintain the balance between updates of A and ϕ fields. Earlier studies of QCD implementation suggest that one should perform updates of the A field much more frequently than the ϕ fields to minimize autocorrelation times [36]. In our simulations ten Metropolis updates of A field follow one heat-bath generation of ϕ fields.

Since the CPU cost is expected to be at least proportional to the number of fields n it is important to adjust this number carefully. One sees from the Eq. (55) that to decrease ϵ one has to increase n to keep the error of approximation constant. In the case of the approximation of the determinant of the matrix $Q^\dagger Q$ one can easily guess that the most economic choice of ϵ should be comparable to the smallest eigenvalue of the matrix $Q^\dagger Q$. To make this discussion more precise we introduce as a measure

$\lvert R_{2n}(x)\rvert$	10^{-2}	10^{-3}	10^{-4}
$\epsilon = 0.003$	26	34	45
$\epsilon = 0.001$	41	60	78
$\epsilon = 0.0005$	59	84	110

Table 1: The number of fields needed to achieve different levels of relative errors $|R_{2n}(x)|$ on the interval $(\epsilon, 1)$

of the error of the polynomial approximation the quantity [37]

$$\delta = |y^{1/V} - 1| \tag{65}$$

with

$$y = \det\left(Q^\dagger Q P_n(Q^\dagger Q)\right) \tag{66}$$

The power $1/V$ properly normalizes the quantity y per one degree of freedom. Fig. 2 shows δ as a function of ϵ for few numbers of fields measured on one typical configuration and confirms simple expectations ($\lambda_{min} = 0.0032$). With this hint we estimated the number of fields n to be about 50-100. This guaranteed that the relative error $|R_{2n}|$ was smaller than 10^{-4} in the whole interval $(\epsilon, 1)$. If one accepts bigger relative errors, for example 10^{-2} these numbers can be reduced but in this case we found discrepancies between exact algorithm and Lüscher implementation (Table.1).

5.2 Dynamical properties of the Lüscher algorithm and its modifications

In order to establish the computational effort required to generate one uncorrelated (independent) statistical event we studied the integrated autocorrelation times for different observables. Let $\{O_t\}(t = 1, \ldots, N_s)$ be an ordered sequence of data produced by our algorithm with the mean value μ. We define the unnormalized autocorrelation function

$$C(t) = \langle O_s O_{s+t} \rangle - \mu^2, \tag{67}$$

normalized autocorrelation function

$$\rho(t) = C(t)/C(0), \tag{68}$$

and integrated autocorrelation time

$$\tau_{int} = \frac{1}{2} \sum_{t=-\infty}^{\infty} \rho(t). \tag{69}$$

The integrated autocorrelation time controls the statistical error of the sample mean

$$\hat{\mu} = \frac{1}{N_s} \sum_{t=1}^{N_s} O_t. \tag{70}$$

Indeed its variance can be rewritten for sufficiently large samples as

$$var(\hat{\mu}) = \langle(\hat{\mu}-\mu)^2\rangle = \frac{1}{N_s^2}\sum_{r,s=1}^{N_s} C(r-s) \simeq \frac{1}{N_s}\sum_{t=-\infty}^{\infty} C(t) = \frac{1}{N_s}\, 2\tau_{int} C(0). \quad (71)$$

Therefore the $2\tau_{int}$ is the number of iterations needed to produce one uncorrelated estimate for O.

Obviously in real situation the estimation of τ_{int} have to be done from a finite data set. However summation over all available data is misleading since the tail of ρ contains a lot of noise but little signal. Therefore in practice we sum the autocorrelations only up to a certain distance T_{cut}

$$\tau_{int}(T_{cut}) = \frac{1}{2} + \sum_{t=1}^{T_{cut}} \rho(t). \quad (72)$$

There are two limitations. If T_{cut} is too large our estimator is very noisy since its variance is

$$var(\tau(T_{cut})) = \frac{2(2T_{cut}+1)}{N_s}\tau_{int}^2. \quad (73)$$

On the other hand two small value of T_{cut} introduces a significant bias. The optimal value of T_{cut} can be easily estimated from sufficiently long runs by the "window" procedure [38]. The recipe is simple: choose T_{cut} to be the smallest integer such that $T_{cut} \geq c\tau_{int}(T_{cut})$. Assuming pure exponential behaviour of $\rho(t) = e^{-t/\tau_{int}}$ it is sufficient to take $c = 4$. Then the bias of our estimator is of order of $e^{-4} = 2\%$.

We have calculated the autocorrelation times for two observables: the average density of electrons with spin up $\langle n_{i\uparrow}\rangle$, and that of pairs of electrons with the opposite spins on the same site $\langle n_{i\uparrow} n_{i\downarrow}\rangle$. The simple updating scheme described above gives large autocorrelation times already for $K = 1$ and $\beta = 1$. It is important to learn whether the long autocorrelations appear while generating ϕ fields or during update of the A field. We have introduced some modifications to the algorithm to address this question.

One could think that these correlations are caused mainly by the critical slowing down introduced by ϕ fields, especially those with small β_k. This would suggest that one would get a better algorithm efficiency by improving updating of the gaussian sector. There are many efficient techniques used in simulations of the gaussian fields. Among them the Multigrid algorithm eliminates completely critical slowing down in the pure gaussian model and therefore we decided to use it to update ϕ fields in our problem [34] [39]. In this approach one considers the sequence of coarse-grid problems which approximate original problem on different length scales and the local updates of the heat-bath algorithm are supplemented by collective updates. We define the set of blocks B_i. For cubic lattice the blocks are taken successively to be single sites (B_0), cubes of side 2 (B_1), cubes of side 4 (B_2) and so on. Obviously if the lattice size is not a power of 2 we can choose also other small blocking factor. With every block we associate the conditional probability distribution, which for

Table 2:

	$\beta=1$, $U=1$ lattice 5^3	$\beta=1$, $U=1$ lattice $6^2 8$	$\beta=1$, $U=2$ lattice $6^2 8$	$\beta=1$, $U=2$ lattice $6^2 14$
Exact determinant	0.460(2)	0.473(2)	0.462(4)	0.468(5)
	0.2197(2)	0.2203(4)	0.195(1)	0.193(1)
	$\tau_1 = 3$	$\tau_1 = 3$	$\tau_1 = 3$	$\tau_1 = 2$
	$\tau_2 = 1.5$	$\tau_2 = 1.5$	$\tau_2 = 1.5$	$\tau_2 = 1$
Simple program	0.461(5)	0.471(6)	—	—
	0.2180(8)	0.221(1)		
	$\tau_1 = 660$	$\tau_1 = 870$		
	$\tau_2 = 320$	$\tau_2 = 300$		
Simple program	—	0.470(4)	—	—
with MG (W-cycle)		0.2194(6)		
		$\tau_1 = 160$		
		$\tau_2 = 80$		
Global generation	0.449(7)	—	—	—
of gaussian fields	0.221(1)			
	$\tau_1 = 180$			
	$\tau_2 = 90$			
Simple program	—	0.470(5)	0.463(7)	0.475(7)
with preconditioning		0.220(1)	0.195(1)	0.186(3)
		$\tau_1 = 100$	$\tau_1 \simeq 200$	$\tau_1 \simeq 600$
		$\tau_2 = 60$	$\tau_2 \simeq 200$	$\tau_2 \simeq 600$

The results for density of electrons $\langle n_{i\uparrow}\rangle$ (first line) and density of pairs $\langle n_{i\uparrow}n_{i\downarrow}\rangle$ (second line). The autocorrelation times are given for both quantities. Autocorrelation times for exact numerical evaluation of the determinant are of the order of unity.

the $\phi_k^{(r)}$ field reads

$$P_B(t) \propto \exp\left[-\sum_{i,j}(\phi_{k,i}^{(r)} + t\,(\chi_B)_i)\left[(Q^\dagger Q - \alpha_k)^2 + \beta_k^2\right]_{i,j}(\phi_{k,j}^{(r)} + t\,(\chi_B)_j)\right]. \quad (74)$$

χ_B denotes the vector whose components are 1 for sites belonging to the block B and 0 elsewhere. The P_B depends only on one real number t.

This general set up can be directly used in our problem as follows. We begin with elementary sites for which we perform the full heat-bath sweep through the lattice sequentially updating $\phi_{k,i}^{(r)}$ for all i, k and r. Then we organize the lattice into blocks B_1. We change the $\phi_{k,i}^{(r)}$ at all sites of given block by the same t according to distribution (74). After having done the sweep over blocks B_1, for all k and r we repeat the same for blocks B_2 and so on. This updating scheme is called V-cycle. The sweeps can be also organized in such fashion that there are γ^l updates of blocks B_l. The control parameter γ defines different classes of MG algorithm. The most common choices are $\gamma = 1$ (V-cycle) and $\gamma = 2$ (W-cycle)

Indeed the MG generation of ϕ fields reduces the autocorrelation times substan-

tially (third row of Table 2). However it introduces additional computational cost. In fact the CPU time required to get one independent sample is even bigger than for a simple heat-bath method. The maximal decorrelation of auxiliary fields is achieved by the independent generation of the eigenmodes. This requires the solution of set of linear equations for each field ϕ and the results are comparable to the MGMC case with W-cycle (4-th row of Table 2).

Neither simple version nor MG refinement is capable to reproduce the exact determinant results for $U = 2$. The system did not thermalize even after 20 times more thermalization steps than required for $U = 1$. This fact can be simply understood. When U increases the condition number of $M^\dagger M$ becomes bigger and larger number of ϕ fields in polynomial approximation is needed. Additionally they are stronger coupled to the A field because of the presence of factor $\exp\sqrt{U\beta/N_t}$. The constraints imposed by large number of ϕ fields on one A field becomes more restrictive and the mobility of algorithm rapidly decreases. Performing updates of A field more frequently is only a partial solution.

Better results gives the preconditioning of fermionic matrix. We define the preconditioning procedure as follows. Let D be a diagonal part of $M = A + D$. Then the matrix $M^\dagger D^{-1} M$ is better conditioned than $M^\dagger M$ as can be seen from Fig. 3 . The effect is clearly visible in the last row of Table 2. As a consequence wider range of couplings become available. However the reliable runs at U greater than 2 are not feasible.

The program based on exact evaluation of determinant has no such restrictions and works equally good at $U = 1$ like for $U = 4$. Required CPU time needed for both algorithms varies with lattice sizes. On small lattices algorithm based on exact evaluation of determinant is substantially faster and it took 20 minutes on HP735/125 workstation to obtain the results on lattice $6^2 8$ while comparing with 10 hours for Lüsher implementation. Of course for larger lattices the computational effort grows much more faster for exact algorithm. In the region of weak coupling and high temperatures we were able to perform simulations on lattices $16^2 \times 8$ with the help of the Lüscher algorithm.

The polynomial approximation can be extended simply to the complex plane [40] [37] i. e. for nonhermitian matrices. Thus one tries to approximate directly the inverse of matrix M. This would reduce the condition numbers for matrices entering the problem and would result in the simpler final action. This modification of original Lüscher idea gave very promising results [37] [46]. However in contrast to the QCD case the matrix M for the Hubbard Model has eigenvalues with the positive as well with negative real parts as can for example be seen on Fig. 4 . Because one cannot extend the domain of the applicability of Eq. (54) beyond the singular point $(0, 0)$, it is unfortunately impossible to adapt this modification to the Hubbard Model.

On the other hand we have found that one change the positions of eigenvalues by introducing the chemical potential. In fact we managed to shift all eigenvalues of the matrix M in simulations of the *attractive* Hubbard Model to the right half of the complex plane. However it occurred at large μ which corresponds to the physically

uninteresting filling ($\langle n_\uparrow + n_\downarrow \rangle > 0.9$).

Other improvements of the Lüscher algorithm have been proposed. Global Metropolis step [41] makes the algorithm exact and heat-bath generation of ϕ fields with overrelaxation slightly reduce autocorrelation times (for review see [42]). We believe however that it would not change the situation qualitatively.

5.3 Magnetic properties of the Hubbard Model

In section 2 we argued for the existence of the antiferromagnetic order in the ground state of the Hubbard Model. These arguments were based on the mean-field approximation and should be independently confirmed in the numerical simulations. In fact, the mean field theory is known to overestimate the magnetic ordering and to underestimate quantum fluctuations. The situation is rather complicated since the Hubbard Model has continuous (spin - SU(2)) symmetry. In that case, in $2d$, the Mermin-Wagner [43] [44] theorem prevents the existence of the long–range magnetic order at finite temperature. The correlation length can become really infinite only at zero temperature when thermal fluctuations vanish.

Therefore to address the problem of magnetic properties of the Hubbard Model it is necessary to perform simulations at large β. This in turn requires sufficient N_t in the discretized form of the path integral formulation to reduce the systematic errors of order of $(\beta/N_t)^2$. Moreover in our particular representation the number of electrons with spin down and with spin up differ. It is special inconvenience in measurements some correlation functions leading to the errors which are extensive function of the lattice size.

To estimate the temperature we can reach, in the physical units we assume that $8K = 1eV$. Then it follows from Eq. (2) that $\beta = 5$ and $K = 1$, the most typical values for our runs correspond to temperature $T = \frac{1}{40}eV = 290$ Kelvin degrees. It would be difficult to reach much lower temperatures due to computer restrictions and finite N_t effects.

We begin discussion with a local quantity which can be simply measured on small lattices with good accuracy. The average number of pairs with opposite spins $\langle n_\uparrow n_\downarrow \rangle$ on the same site shows how repulsive interaction forbids double occupancy of a site. Clearly increasing U leads to reduction in number of pairs. Fig. 5 compares results from QMC simulations with the mean field prediction. The derivation of the latter is presented in the Appendix A. Here we note a good qualitative agreement with MC results. For this quantity a 4×4 lattice gives rather good approximation to the bulk result and we did not notice meaningful finite size effects as can be seen from Table.3 .

To decide weather the ground state has the long range antiferromagnetic order one can attempt to measure the equal time correlations between magnetization on different sites

$$C(l_x, l_y) = \langle (n_{i\uparrow} - n_{i\downarrow})(n_{i+l\uparrow} - n_{i+l\downarrow}) \rangle. \tag{75}$$

This quantity obtained form simulations on 4×4 lattice at $\beta = 5$ and $U = 4$ is shown

$\langle n_{i\uparrow} n_{i\downarrow} \rangle$	N=16	N=36	N=64	N=100	N=144
$U = 1\ \beta = 1\ N_t = 8$	0.2195(4)	0.2204(4)	0.2202(5)	0.2202(3)	0.2198(3)
$U = 4\ \beta = 5\ N_t = 30$	0.134(2)	0.138(2)			

Table 3: The density of pairs on the same site as a function of the spatial volume of the lattice $N = N_x^2$. For this quantity the lattice 4^2 already gives good approximation to the bulk result

on Fig. 6 . The visible zig-zag is an indication of the onset of the antiferromagnetism. We found that this observable is very sensitive to finite N_t effects. We needed 60 time slices to obtain clear signal (the analogical zig-zags for $N_t = 30$ and $N_t = 40$ do not look so nice). This is not surprising since the inequality between $\langle n_{i\uparrow} \rangle$ and $\langle n_{i\downarrow} \rangle$ is equivalent to putting the system into a magnetic field which destroys the antiferromagnetic correlations. Within the spin wave theory the correlation between two most distant points on the lattice is simply related to the antiferromagnetic order parameter m [45]

$$C(N_x/2, N_x/2) = \frac{m^2}{3} + O(1/N_x) \tag{76}$$

with the finite size corrections of order $O(1/N_x)$ on the lattice with spatial volume $N = N_x^2$. For the parameters of run the mean field result $m^2/3 = 0.15$ should be compared with the value 0.10 ± 0.04 read from Fig. 6 . Thus even for relatively high temperature of our simulations we obtained a good agreement. We did not estimate the finite size effects because it requires the simulations on bigger lattices.

Fourier transformation of $C(l)$ gives the magnetic structure factor

$$S(q) = \sum_{l_x, l_y} \exp{(iql)} C(l) \tag{77}$$

which is especially well suited for detecting excitations with wave vector q. In the presence of antiferromagnetic long-range order we expect divergence of the $S(\pi, \pi)$ with the lattice size according to

$$S(\pi, \pi) = N \frac{m^2}{3} + O(1/N_x). \tag{78}$$

So far no one has shown in direct simulations the existence of antiferromagnetic phase at U below 2 [9]. Since we can reach quite large lattices at small U using the Lüscher method we made such an attempt. Fig. 7 gives the $S(k_x, k_x)$ as a function of momentum on lattices with spatial sizes ranging from 4×4 to 16×16 for $\beta = 1$ and $U = 1$. Within the statistical errors there is no dependence of the magnetic structure factor on lattice volume at this temperature. An exception is $S(0, 0)$ which rises with N almost linearly. It is a simple artefact of finite N_t and does not mean that system has ferromagnetic long range order. Indeed the $S(0, 0)$ is defined as an extensive quantity and naively we can expect the contribution to the $S(0, 0)$ of order of $N(\Delta n)^2$ coming from the difference Δn between $\langle n_\uparrow \rangle$ and $\langle n_\downarrow \rangle$. This crude

	$N_t = 6$	$N_t = 8$	$N_t = 12$
a =	0.33(3)	0.34(2)	0.34(3)
b=	0.044(4)	0.030(2)	0.013(2)
$(\Delta n)^2$	0.041	0.025	0.010

Table 4: Parameters a and b obtained from simulations on lattices with $N_t = 6, 8, 12$. The mean difference $(\Delta n)^2$ is also given.

N=16	N=36
2.6 ± 0.2	3.2 ± 1.0
2.8	4.2

Table 5: Comparison of results for $S(\pi, \pi)$ obtained from our studies (first row) with those from Ref. [12] (second row).

estimation is tested in Fig. 8 where the $S(0,0)$ is shown as a function of the spatial volume of the lattice for $N_t = 6$, $N_t = 8$ and $N_t = 12$. For each N_t we found the parameters of linear fit

$$S(0,0) = bN + a \tag{79}$$

The results are listed in Table 4. The values of b should be compared with the mean difference $(\Delta n)^2$. The remaining contribution a, which does not depend on N_t may be regarded as a true $S(0,0)$. The nonozero value of $S(0,0)$ is an effect of the short-range correlations.

The simulations described above were performed at rather high temperature (corresponding $\beta = 1$). We did not found the antiferromagnetism because of the disordering effect of thermal fluctuations. We performed some simulations with the help of the exact algorithm at $U = 4$ and the $\beta = 5$ where the scaling predicted by the Eq. (78) has been observed [12]. Due to strong finite N_t effects to obtain valid result one has to perform extrapolation. The finite N_t errors introduced by our lattice discretization are of the order of $(\frac{\beta}{N_t})^2$. In Fig. 9 we present $S(\pi, \pi)$ as a function of parameter $(\frac{\beta}{N_t})^2$. In the limit $1/N_t \to 0$ for the lattice 4×4 we obtained 2.6 ± 0.2 and for the lattice 6×6 3.2 ± 1.0. They compare satisfactorily with MC simulations of Ref. [12] (see Table. 5).

5.4 Fermi surface

It is also very interesting to study information contained in one particle finite temperature Green's function defined in the momentum space and imaginary time as

$$G(k, \tau) = -\langle T a_{k\sigma}(\tau) a^{\dagger}_{k\sigma}(0) \rangle, \tag{80}$$

where $a(\tau)$ is the annihilation operator in the Heisenberg picture and T time ordering operator. The limit of $G(k, \tau \to 0^-)$ has simple physical content. It gives

distribution of electrons in the momentum space. To see the shape of the Fermi surface one has to perform simulations on sufficiently large lattices. The largest lattice accessible to our simulations was $8^2 \times 20$. For the parameters of run $U = 4$ and $\beta = 5$ the number of time slices might appear too small. However, for this quantity we do not expect the presence of the mechanism described above which leads to the errors which are extensive function of the spatial lattice volume.

Finally, one can also compare our results with the mean-field prediction. It follows from Eq. (95) in Appendix A that

$$n(k) = n_{k\downarrow} + n_{k\uparrow} = 1 - \frac{\epsilon_k}{\sqrt{\epsilon_k^2 + \Delta^2}} \tag{81}$$

The energy gap $\Delta = 1.38$ is almost the same for the lattice 6×6 and for the lattice 8×8. Consequently we can together compare results from lattices 6×6 and 8×8 with the mean field formula (solid line in Fig. 10). Even for our relatively large $\beta/N_t = 0.25$ the results we obtained are in a good agreement with the theoretical prediction. However the Fermi surface of the interacting system is more smooth than in the noninteracting case (dotted line). Obviously this effect is an increasing function of U.

The lack of sharp Fermi surface suggests vanishing Z and behaviour different from the Fermi liquid. Of course it would be very interesting to measure the $n(k)$ at non zero chemical potential μ and find the critical value μ_{crit} when the sharp Fermi surface appears. Unfortunately the QMC simulations are not conclusive at small μ due to sign problem. Currently it is only confirmed that μ_{crit} is small.

5.5 Effective hopping

As pointed out in various approximate schemes the interaction leads to the reduction in the effective hopping. In our Monte Carlo simulations we measured the ratio

$$\frac{K_{eff}}{K_0} = \frac{\langle a^\dagger_{i\sigma} a_{j\sigma} \rangle_U}{\langle a^\dagger_{i\sigma} a_{j\sigma} \rangle_0}, \tag{82}$$

which shows how interaction reduces the effective hopping matrix elements between nearest neighbor sites i, j. This quantity can be measured directly or can be expressed in terms of Green's function. Indeed K_{eff} can be written as an expectation value over the whole lattice

$$K_{eff} = \frac{1}{4N} \langle \sum_{x,\nu} a^\dagger_x a_{x+\nu} + h.c \rangle, \tag{83}$$

where x denotes the sites on the lattice, ν is the unit versor and N is spatial volume of the lattice. For simplicity we drop the spin index. Replacing the operators a_x by their Fourier transforms yields

$$\begin{aligned} K_{eff} &= \frac{1}{4N^2} \sum_{k,k',\nu} \langle a^\dagger_{k'} a_k \rangle (e^{ik\nu} + e^{-ik'\nu}) \sum_x e^{i(k-k')x} \\ &= -\frac{1}{4N} \sum_k \langle a^\dagger_k a_k \rangle \epsilon_k \end{aligned} \tag{84}$$

Finally

$$K_{eff} = -\frac{1}{4N}\sum_k n(k)\epsilon_k. \tag{85}$$

The last equation is very convenient since the mean field formula for $n(k)$ has been already given. In Fig. 11 we compare the results from simulations and the mean-field prediction. The observed reduction is smaller than given by the theory. It is not surprising since the mean field approximation is known to *overestimate* effect of U. Indeed the mean field ground state does not take into account the suppression of double occupancy. Consequently the effect of the interaction term is overestimated.

6 Summary and conclusions

Motivated by the interest for numerical approach proposed by Lüscher we have developed a Monte Carlo algorithm for studying the two dimensional Hubbard Model. Our method is based on the field theoretical formulation in $(2+1)$ dimensions, to which we applied the polynomial approximation proposed by Lüscher [2]. Finally we obtained the local action and therefore we were able to study the system using bosonic techniques. We have introduced a number of improvements which reduce the long autocorrelation times. In particular we show that by introducing a preconditioning of the fermionic speeds up the algorithm significantly. We have also compared the efficiency of the Lüscher algorithm with the simple algorithm based on the direct update of the determinant of the fermionic matrix. It follows from this comparison that at present stage Lüscher technique does not seem to be a true alternative to the standard simulations of the Hubbard Model. The Lüscher method can not reach the most interesting region of strong coupling because then the fermionic matrices are very badly conditioned, much more worse than in the case of QCD. A large number of the additional bosonic fields is required and the algorithm suffers from strong autocorrelations. Another difficulty arises from nonhermicity of the fermionic matrix of the Hubbard Model which complicates the resulting action and squares the condition numbers for matrices entering the problem. The nonhermitian version of the Lüscher algorithm can not be also applied.

The algorithm based on the direct update of the determinant of the fermionic matrix was modeled after the algortihm from Ref. [11]. However we found that numerical instabilities do not appear in our particular representation of path integrals, which allow to avoid additional complications. Hence we managed to reach region of strong coupling and quite large β at half-filling with the help of this very simple algorithm. Whenever it was possible we also compared our results with results of previous investigations as well with the mean field theory.

To show the that the ground state has antiferromagnetic long range order we measured the correlation between two different sites on the lattice. We found that main limitations in measurements of this quantity are finite N_t effects which introduce significant bias. Nevertheless, through the extrapolation $N_t \to \infty$, we were able to obtain results which are in a qualitative agreement with other QMC simulations [11] [12]. We have also attempted to measure the one-particle properties. In

particular we showed that the Fermi surface is not sharp with the shape described well by the mean-field theory. This shows that the system is in the insulating Neel state. Thus we did not found any unexpected behavior and our results confirm the often presented opinion that the physics of the half-filled Hubbard Model is well understood.

On the other hand there is the case of non half-filled band with possible existence of the superconducting phase. Although the Projector Quantum Monte Carlo simulations delivered substantial progress in this field the situation still remains unclear. Especially just below the half-filling where the sign problem is a serious obstacle. Current simulations are consistent with the most orthodox point of view treating holes as quasiparticles but other non Fermi liquid scenarios are not completely excluded [4] [12] [14]. It is also impossible to make final conclusions about existence of the superconducting phase because the range of parameters accessible to simulations is too narrow.

Acknowledgments

I would like to specially thank my thesis advisor J. Wosiek for the continuous interest in my work, helpful comments and discussions. I have benefited also from discussions with Z. Burda and K. Rościszewski. I am very grateful to the Foundation for Polish Science for the fellowship. The work was partially supported by the KBN grants no. 2P03B19609 and no. 2P03B04412. The nuumerical calculations were partly performed at the ACK Cyfronet-Kraków. Computational grant: KBN/UJ/055/94.

A Appendix A

In this Appendix we apply the mean field theory [47] to the half-filled Hubbard Model on the square lattice with the antiferromagnetic order in the ground state. Within this approximation one rewrites the operator of the number of electrons at a given site i as $n_{i\sigma} = \langle n_{i\sigma}\rangle + (n_{i\sigma} - \langle n_{i\sigma}\rangle)$ where $\langle n_{i\sigma}\rangle$ is the expectation value in the ground state. Then assuming the fluctuations to be small, the interaction term in Hamiltonian becomes

$$n_{i\uparrow}n_{i\downarrow} = -\langle n_{i\uparrow}\rangle\langle n_{i\downarrow}\rangle + n_{i\uparrow}\langle n_{i\downarrow}\rangle + n_{i\downarrow}\langle n_{i\uparrow}\rangle \tag{86}$$

It is convenient to choose as the ground state Spin Density Wave (SDW) state defined by

$$\langle n_{i\uparrow}\rangle = \frac{1}{2}\left[1 + m(-1)^i\right], \;\; \langle n_{i\downarrow}\rangle = \frac{1}{2}\left[1 - m(-1)^i\right] \tag{87}$$

where as usual $(-1)^i \equiv (-1)^{i_x+i_y}$ is the parity of site, and m is a variational parameter. Its value will be determined from the minimum energy condition. Note that we are able to reproduce the result for interacting electrons putting $m = 0$ and the antiferromagnetic Neel state ($m = 1$). Transformation of the original Hamiltonian to the momentum space yields the mean field Hamiltonian in the form

$$\mathcal{H}_{MF} = \sum_{k\sigma}\epsilon_k a^\dagger_{k\sigma}a_{k\sigma} - \frac{Um}{2}\sum_k (a^\dagger_{p+Q\uparrow}a_{k\uparrow} + a^\dagger_{p+Q}a_{k\downarrow}) + N\frac{Um^2}{4}. \tag{88}$$

where $\epsilon_k = -2K(\cos k_x + \cos k_y)$ are the bare energy levels and $Q = (\pi, \pi)$. The above Hamiltonian is diagonal in the spin indices and the operators with momentum k can interact only with those of momentum $k + Q$. Thus our problem reduces to the diagonalization of the set of matrices

$$\begin{pmatrix} \epsilon_k & \pm mU/2 \\ \pm mU/2 & \epsilon_{k+Q} \end{pmatrix}. \tag{89}$$

The eigenvectors and eigenvalues can now be simply obtained

$$\begin{aligned} \gamma^{(+)}_{k\uparrow} &= u_k a_{k\uparrow} - v_k a_{k+Q\uparrow}, \;\; \gamma^{(+)}_{k\downarrow} = u_k a_{k\downarrow} + v_k a_{k+Q\downarrow}, \\ \gamma^{(-)}_{k\uparrow} &= v_k a_{k\uparrow} + u_k a_{k+Q\uparrow}, \;\; \gamma^{(-)}_{k\downarrow} = v_k a_{k\downarrow} - u_k a_{k+Q\downarrow}. \end{aligned} \tag{90}$$

There are two eigenvectors per spin and momentum k is in the reduced Brillouin zone. The transformation amplitudes u_k and v_k are

$$\begin{aligned} u_k^2 &= \frac{1}{2}\left(1 + \frac{\epsilon_k}{E_k}\right), \\ v_k^2 &= \frac{1}{2}\left(1 - \frac{\epsilon_k}{E_k}\right), \\ E_k &= \left(\epsilon_k^2 + \Delta^2\right)^{1/2}, \\ \Delta &= -\frac{mU}{2}. \end{aligned} \tag{91}$$

where Δ is the energy gap parameter and $\pm E_k$ are the eigenvalues of $\gamma_k^{(\pm)}$. At the edge of the Fermi surface $k = (-\pi/2, \pi/2)$ we have two possible energies $E = \pm\Delta$ thus the system acquires gap equal 2Δ. The mean field ground state is obtained by filling the states with lower energy (i.e. those with the sign (-) in front of E_k).

$$|\psi_{MF}\rangle = \prod_{|k|\leq k_F} (\gamma_{k\uparrow}^{(-)})^\dagger (\gamma_{k\downarrow}^{(-)})^\dagger |0\rangle, \tag{92}$$

with the empty state denoted by $|0\rangle$. The condition for energy minimum leads to the self-consistent equation for the energy gap

$$\frac{1}{U} = \frac{1}{N} \sum_{|k|\leq |k_F|} \frac{1}{(\epsilon_k^2 + \Delta^2)^{1/2}} \tag{93}$$

where the sum over momenta is restricted to half of Brillouin zone (k_F is the momentum at the noninteracting Fermi surface). The above equation for Δ for finite lattices can be easily solved numerically. The mean field predictions can be simply obtained for physically interesting quantities. For example the double occupancy of the site is simply related to the antiferromagnetic order parameter m

$$\langle n_{i\uparrow} n_{i\downarrow}\rangle = \langle n_{i\uparrow}\rangle\langle n_{i\downarrow}\rangle = \frac{1}{4}(1 - m^2). \tag{94}$$

One can also obtain the occupation number in the momentum space

$$n_{k\sigma} = \langle \psi_{MF}| a_{k\sigma}^\dagger a_{k\sigma} |\psi_{MF}\rangle = \frac{1}{2}\left(1 - \frac{\epsilon_k}{E_k}\right). \tag{95}$$

Indeed the electrons with momentum k are created from the state $|0\rangle$ with the amplitude v_k, given by Eq. (91) if the momentum k lies inside the Fermi surface. Similarly the electrons outside the Fermi surface are created with the amplitude $u_{k-Q} = v_k$.

B Appendix B

In this Appendix we review the formalism of Grassmann variables [17] [18]. A set of anticommuting Grassmann variables is defined by the relation

$$[\psi_i, \psi_j]_+ \equiv \psi_i\psi_j + \psi_j\psi_i = 0. \tag{96}$$

For each ψ_i there is also corresponding independent variable $\psi_i^\star$. Moreover we have

$$\begin{aligned} (\psi_i^\star)^\star &= \psi_i \quad , \\ (\psi_1 \cdots \psi_n)^\star &= \psi_n^\star \cdots \psi_1^\star \quad . \end{aligned} \tag{97}$$

Assuming the properties of linearity and invariance under translation of variables the integration can be defined through the formulas

$$\begin{aligned} \int d\psi\, \psi &= i \\ \int d\psi\, 1 &= 0 \\ \int d\psi^\star\, d\psi\, \psi^\star\, \psi &= 1. \end{aligned} \tag{98}$$

Since the general function of Grassmann variables is in fact polynomial the above equations are sufficient to compute any integral. In addition to integration we consider the differentiation with the respect to the Grassmann variable. This can be defined by the action on a constant function and an anticommutation relation

$$\frac{d}{d\psi}1 = 0 \quad , \left[\frac{d}{d\psi^\star}, \psi^\star\right]_+ = 1. \tag{99}$$

Function of Grassmann variables form the Hilbert space on which transfer matrix acts. To make this statement more specific we consider as an example the case of one degree of freedom. Then one can relate the function $f(\psi^\star) = 1$ to the vacuum state $|0\rangle$ and the function $f(\psi^\star) = \psi^\star$ to the occupied state $|1\rangle$. The operators $a^\dagger$ and a would correspond to $\psi^\star$ and $\frac{d}{d\psi^\star}$ respectively.

It is convenient to introduce the simple analog of Dirac δ function for the anticommuting variables

$$\delta(\psi^\star, \psi'^\star) = \int (d\psi) e^{\sum (\psi^\star - \psi'^\star)\psi}, \tag{100}$$

where $(d\psi)$ denotes $\prod d\psi_i$ in some prescribed order. Note that the δ function has the expected property

$$f(\psi^\star) = \int \delta(\psi^\star, \psi'^\star)(d\psi')^\star f(\psi'^\star). \tag{101}$$

Now it is easy to verify the correspondence on the level of integral representations for operators acting on a general state $|f\rangle$

$$\begin{aligned} a_i|f\rangle &\leftrightarrow \int \psi_i \, (d\psi) e^{\sum (\psi^\star - \psi'^\star)\psi} \, (d\psi')^\star f(\psi'^\star) \, , \\ a_i^\dagger|f\rangle &\leftrightarrow \int \psi_i^\star \, (d\psi) e^{\sum (\psi^\star - \psi'^\star)\psi} \, (d\psi')^\star f(\psi'^\star) \, . \end{aligned} \tag{102}$$

The result is very simple and states that under integral a and $a^\dagger$ should be replaced by ψ and $\psi^\star$ respectively. This immediately generalizes to any normal ordered function of a and $a^\dagger$

$$: g(a^\dagger, a) : |f\rangle \leftrightarrow \int g(\psi^\star, \psi) \, (d\psi) e^{\sum (\psi^\star - \psi'^\star)\psi} \, (d\psi')^\star f(\psi'^\star). \tag{103}$$

It is very important that the function g is normal ordered. Variables ψ and $\psi^\star$ simply anticommute while the anticommutation relation between $\psi^\star$ and $\frac{d}{d\psi^\star}$ introduces additional factors.

The trace of a normal ordered operator can be rewritten in the form of integral over anticommuting variables

$$Tr \ : g(a^\dagger, a) : = \int (d\psi)^\star g(\psi^\star, \psi) e^{2 \sum \psi^\star \psi} (d\psi). \tag{104}$$

A little algebra yields the trace of normal ordered factors as a multiple integral over anticommuting variables

$$\begin{aligned} Tr[: g_1(a^\dagger, a) :: g_2(a^\dagger, a) : \cdots : g_{N_t}(a^\dagger, a) :] = \\ \int \prod_{t=1}^{N_t} [(d\psi_t)^\star g_t(\psi_t^\star, \psi_t)(d\psi_t) e^{\sum \psi_t^\star (\psi_t - \psi_{t-1})}], \end{aligned} \tag{105}$$

with antiperiodic boundary conditions $\psi_0 = -\psi_{N_t}$. For operators g being the transfer matrices of the Hubbard Model the integration is performed by the standard formula

$$\int (d\psi)^\star \, (d\psi) e^{\psi^\star M \psi} = \det M. \tag{106}$$

which directly gives Eq. (23).

The expectation value of observables just inserts another factor in the above integral. The additional factors under integral are

$$\int (d\psi_{N_t+1})^\star \, (d\psi_{N_t+1}) \, h(\psi^\star_{N_t+1}, \psi_{N_t+1}) \exp\left[\psi^\star_{N_t+1}(\psi_{N_t+1} - \psi_{N_t}) + \psi^\star_1(\psi_{N_t+1} - \psi_{N_t})\right]. \tag{107}$$

As an example we consider the expectation value for the numbers of electrons with spin up and the corresponding function : $h(a^\dagger, a) := a^\dagger a$. Then the integration over additional factors reduces simply to the insertion $1 - \psi^\star_1 \psi_{N_t}$ under the main integral. The evaluation of integral of such type is simple if we make use of the identity

$$\int (d\psi)^\star d\psi e^{\psi^\star M \psi + \xi\psi + \psi^\star \eta} = \det M \; e^{-\xi M^{-1} \eta}. \tag{108}$$

The additional factors can be obtained simply by differentiation with the respect to the anticommuting variables η and ξ next putting them zero. In our example

$$\int (d\psi)^\star \, (d\psi) e^{\psi^\star M \psi} \;\; (1 - \psi^\star_{i,1} \psi_{i,N_t}) = \det M \quad (1 - M^{-1}_{i,N_t;i,1}). \tag{109}$$

Cyclically shifting in t direction yields

$$\langle n_{i\uparrow} \rangle = \langle 1 + M^{-1}_{i,t;i,t+1} \rangle. \tag{110}$$

In similar derivation for the electrons with spin spin down one should first perform the particle hole transformation $a^\dagger_\downarrow a_\downarrow = b b^\dagger = 1 - b^\dagger b$. The corresponding insertion is $\psi^\star_1 \psi_{N_t}$ and the final result reads

$$\langle n_{i\downarrow} \rangle = -\langle M^{-1}_{i,t;i,t+1} \rangle. \tag{111}$$

Similar considerations give the expressions for the other observables of interest

$$\begin{aligned}
\langle n_{i\uparrow} n_{i\downarrow} \rangle &= -\langle M^{-1}_{i,t;i,t+1}(1 + M^{-1}_{i,t;i,t+1}) \rangle & (112)\\
C(i,j) &\equiv \langle (n_{i\uparrow} - n_{i\downarrow})(n_{j\uparrow} - n_{j\downarrow}) \rangle \\
C(i,j) &= \langle 1 + 2M^{-1}_{i,t;i,t+1} + 2M^{-1}_{j,t;j,t+1} - 2M^{-1}_{i,t;i,t+1}\delta_{i,j} \\
&\qquad + 4M^{-1}_{i,t;i,t+1} M^{-1}_{j,t;j,t+1} - 2M^{-1}_{i,t;j,t+1} M^{-1}_{j,t;i,t+1} \rangle & (113)\\
n(k) &= \frac{1}{N} \sum_{xy} e^{ik(x-y)} \langle M^{-1}_{x,t;y,t+1} - (-1)^x (-1)^y M_{x,t;y,t+1} + \delta_{x,y} \rangle. & (114)
\end{aligned}$$

References

[1] M. Creutz, *"Quarks, Gluons and Lattices"*, Cambridge University Press 1983.

[2] M. Lüscher, Nucl. Phys. **B418** (1994) 637.

[3] J. Hubbard, Proc. Roy. Soc. **A 276** (1963) 238.

[4] E. Dagotto, *"Correlated Electrons in high temperature superconductors"*, Rev. of Mod. Phys. **Vol. 66 No. 3**.

[5] P. W. Anderson, Science **234** (1987) 1196.

[6] E.H.Lieb, F.Y. Wu, Phys. Rev. Lett. **20** (1968) 1445.

[7] E. Fradkin, *"Field theory of condensed matter systems"*, Addison-Wesley Publishing Company 1991.

[8] H. Yokoyama and H. Shiba, J.Phys.Soc.Jpn **56** (1987) 1490;
H. Yokoyama and H. Shiba, J.Phys.Soc.Jpn **56** (1987) 3582.

[9] J. E. Hirsh, S. Tang, Phys. Rev. Lett. **62** (1989) 591

[10] A.L.Fetter, J.D.Walecka, *"Quantum Theory of Many Particle Systems"*, McGraw Hill, 1971.

[11] S.R. White et al., Phys. Rev. **B40** (1989) 506.

[12] D. J. Scalapino, *"Results from Numerical Simulations of the 2D Hubbard Model."* in *"High Temperature Superconductivity Proceedings*, Addison Wesley, 1990.

[13] S.Sorella, Phys. Rev. **B46** (1992) 11670.

[14] D.J.Scalapino, Phys. Rep. **250** (1995) 329.

[15] R. dos Santos, Phys. Rev. **B39** (1989) 7259.

[16] R.T.Scalettar and al., Phys. Rev. Lett. **12** (1989) 1407.

[17] M. Creutz, Phys. Rev. **B38** (1988) 1228.

[18] M. Creutz, Phys. Rev. **D35** (1987) 1460.

[19] J. Wosiek, Acta Phys. Pol. **B18** (1987) 519 and references therein.

[20] F.Fucito, E.Marinari, G.Parisi and C.Rebbi Nucl. Phys. **B 180** (1981) 369.

[21] M. Creutz, *"Algorithms for simulation of fermions"* in *"Quantum Fields on the computer"* , World Scientific, 1992.

[22] G.G.Batrouni, G.R.Katz, A.S.Kronfeld, G.P.Lepage and K.G.Wilson, Phys. Rev. **D32** (1985) 2736.

[23] J.Polonyi and H.W.Wyld, Phys. Rev. Lett. **51** (1983) 2257;
J.Kogut, J.Polonyi, H.W.Wyld and D.K.Sinclair, Phys. Rev. Lett. **54** (1983) 1475.

[24] S. Duane, A.D.Kennedy, B.J.Pendelton and D. Roweth , Phys. Lett. **B195** (1987) 216.

[25] K. Jansen and C. Liu, Nucl.Phys. **B453** (1995) 375.

[26] R. Lacaze, A. Morel, B. Petersson and J. Schroeper, *"An investigation of the 2d attractive Hubbard Model "*, preprint BI-TP 96/05.

[27] J.E.Hirsch, Phys. Rev. **B 31** (1985) 4403.

[28] G.Sugiyama, S.E.Koonin Ann. of Phys. **168** (1986) 1.

[29] S.Sorella, S.Baroni, R.Car, M.Parinello, Europhys. Lett. **8** (1989) 663;
S.Sorella et al. Int. J. Mod. Phys. **1** (1988) 993.

[30] A. Galli, *"Suppresion of the negative sign problem in quantum Monte Carlo"* , hep-lat 9605026.

[31] H.Q.Lin, J.E.Gubernatis, Comp. Phys. **Vol. 7** (1993) 400.

[32] P. Sawicki and J. Wosiek, Nucl. Phys. **B42** (Proc. Suppl.) (1995) 932;
P. Sawicki and J. Wosiek, Nucl. Phys. **B47** (Proc. Suppl.) (1996) 785.

[33] "Numerical Receipes", Cambridge University Press 1986.

[34] A. Sokal *"Monte Carlo Methods in Statistical Mechanics: Foundations and New Algorithms"* , Cours de Troisieme Cycle de la Physique en Suisse Romande.

[35] N. Metropolis et al., J. Chem. Phys. **21**, 1087 (1953).

[36] B. Jegehrlehner, Nucl. Phys. **B42** (Proc. Supll.) (1995);
K. Jansen, C. Liu, B. Jegehrlehner, *"Performance Tests of the Kramers Equation and Boson Algorithms for simulations of QCD"* , preprint DESY95-243.

[37] A. Borici an Ph. de Forcrand, *"Systematic errors of Lüscher's fermion method and its extensions"*, preprint IPS-95-13.

[38] N. Madras, A. Sokal, J. Stat. Phys. **50** (1988) 109.

[39] R. G. Edwards et al. , Nucl. Phys. **B354** (1991) 289.

[40] I. Montvay, *"An algorithm for gluinos on the lattice"*, preprint DESY 95-192.

[41] C. Alexandrou et al. *"Full QCD with the Lüscher local bosonic action"* preprint UCY-PHY-95/5.

[42] S. L. Adler, Phys. Rev. **D37** (1988) 458.

[43] N.D.Mermin and H.Wagner, Phys. Rev. Lett. **17** (1966) 1133.

[44] A. Auerbach, *"Interacting Electrons and Quantum Magnetism"*, Springer-Verlag 1994.

[45] D.A.Huse, Phys. Rev. **B37** (1988) 2380.

[46] Ph. de Forcrand and A. Galli, *"Exact Local Bosonic Algorithm for full QCD"*, hep-lat 9603011.

[47] J. R. Schreiffer, X. G. Wen and S.C. Zhang, Phys. Rev. **B39** (1989) 11663.

Figure Captions

1. Fermi surface for the 2d Hubbard Model on the square lattice. The dashed area corresponds to the occupied states for half-filling.

2. Errors of the Lüscher approximation measured on a single typical configuration genrated at $U = 1$ and $\beta = 1$. The quantity δ defined in text is shown as a function of ϵ. The solid, dashed and dotted line is for number of fields 50, 70 and 100 respectively.

3. The distribution of the condition numbers for the $M^\dagger M$ matrix (solid line) and the preconditioned matrix $M^\dagger D^{-1} M$ (dashed line). Results from simulations on $6^2 \times 12$ lattice at $U = 4$ and $\beta = 1$.

4. Eigenvalues of the matrix M plotted on the complex plane. A typical configuration was taken from simulations at $U = 1$ and $\beta = 1$.

5. The double occupancy versus U on a 4×4 lattice with $\beta = 5$. The solid line is the mean-field result.

6. Magnetic correlation function $C(l)$ on the 4×4 lattice. The point l traces the triangular path shown in the picture. The antiferromagnetic correlations are clearly visible at $N_t = 60$, $\beta = 5$ and $U = 4$. The shape of curve is very sensitive to the finite N_t effects. The results at $N_t = 30$ (dotted line) and $N_t = 40$ (dashed line) are also shown for comparison.

7. Magnetic factor $S(k_x, k_x)$ along the main diagonal of the Brillouin zone. Results from lattices 6×6 (empty circles), 8×8 (triangles), 12×12 (circles) and 16×16 (crosses) are collected. Other parameters of runs were $U = 1$ and $\beta = 1$. There is no signal of long range antiferromagnetic order at this temperature.

8. Finite N_t analysis of antiferromagnetic factor $S(\pi, \pi)$. Its value is extrapolated in the parameter $(\frac{\beta}{N_t})^2$. Results from lattices 4×4 (circles) and 6×6 (triangles) are presented. The extrapolation with $N_t \to \infty$ gives result 2.6 ± 0.2, and 3.2 ± 1.0 respectively.

9. The ferromagnetic factor $S(0, 0)$ as a function of spatial volume of the lattice. Three sets of data are shown for $N_t = 6$ (circles), $N_t = 8$ (triangles), and $N_t = 12$ (crosses).

10. The distribution of electrons $\langle n_{k\uparrow} + n_{k\downarrow} \rangle$ in the momentum space. Monte Carlo results from lattice 6×6 (crosses) and 8×8 (triangles) are shown. They are well described by the mean-field theory (solid line). Dashed line is a noninteracting Fermi distribution $f(\epsilon_k) = 2(\exp(-\beta \epsilon_k) + 1)^{-1}$.

11. The effective hopping versus U on a 4×4 lattice with $\beta = 5$. The solid line is the mean field result.

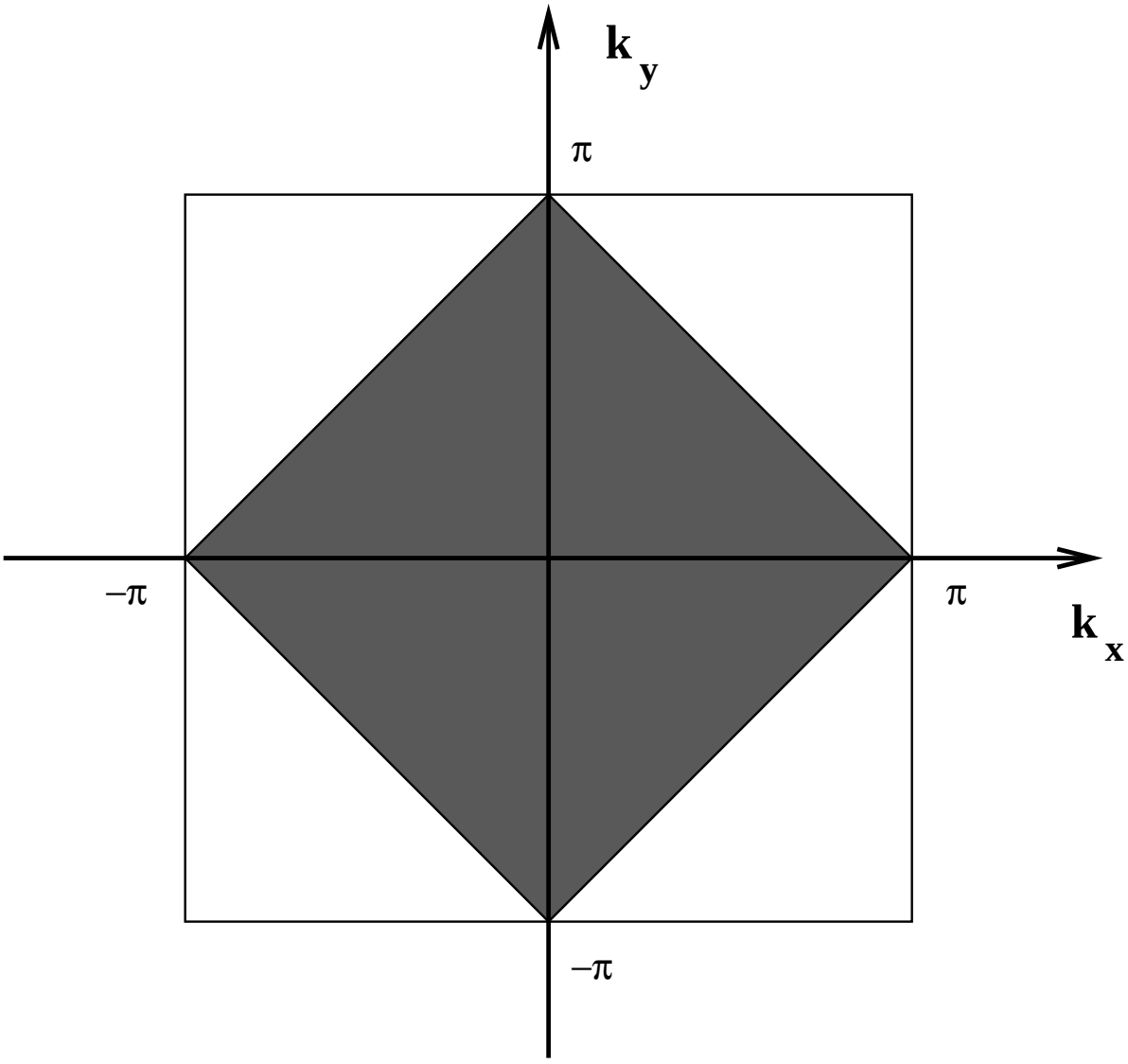

Figure 1:

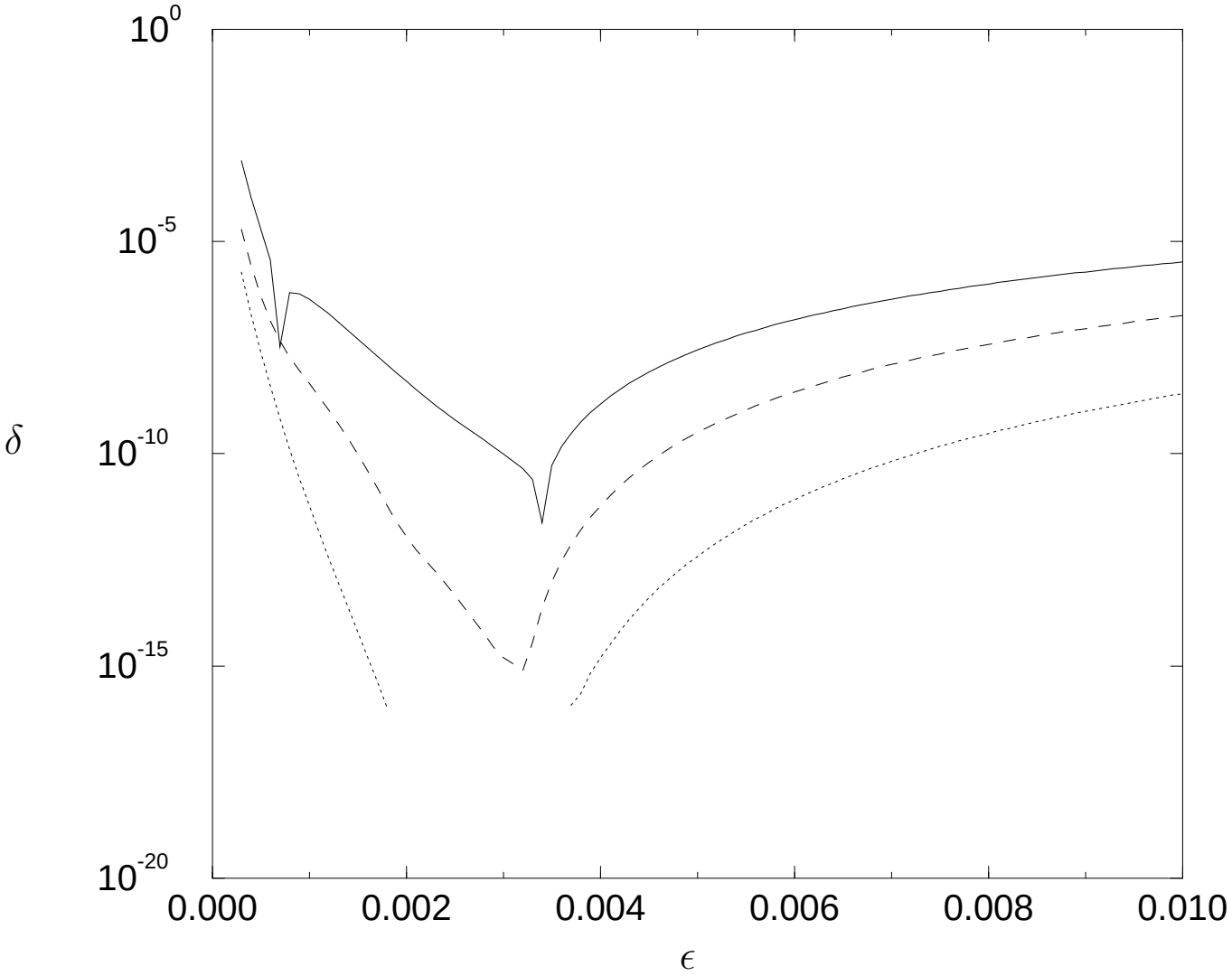
10^0
10^{-5}
10^{-10}
10^{-15}
10^{-20}
δ
0.000
0.002
0.004
0.006
0.008
0.010
ϵ

Figure 2:

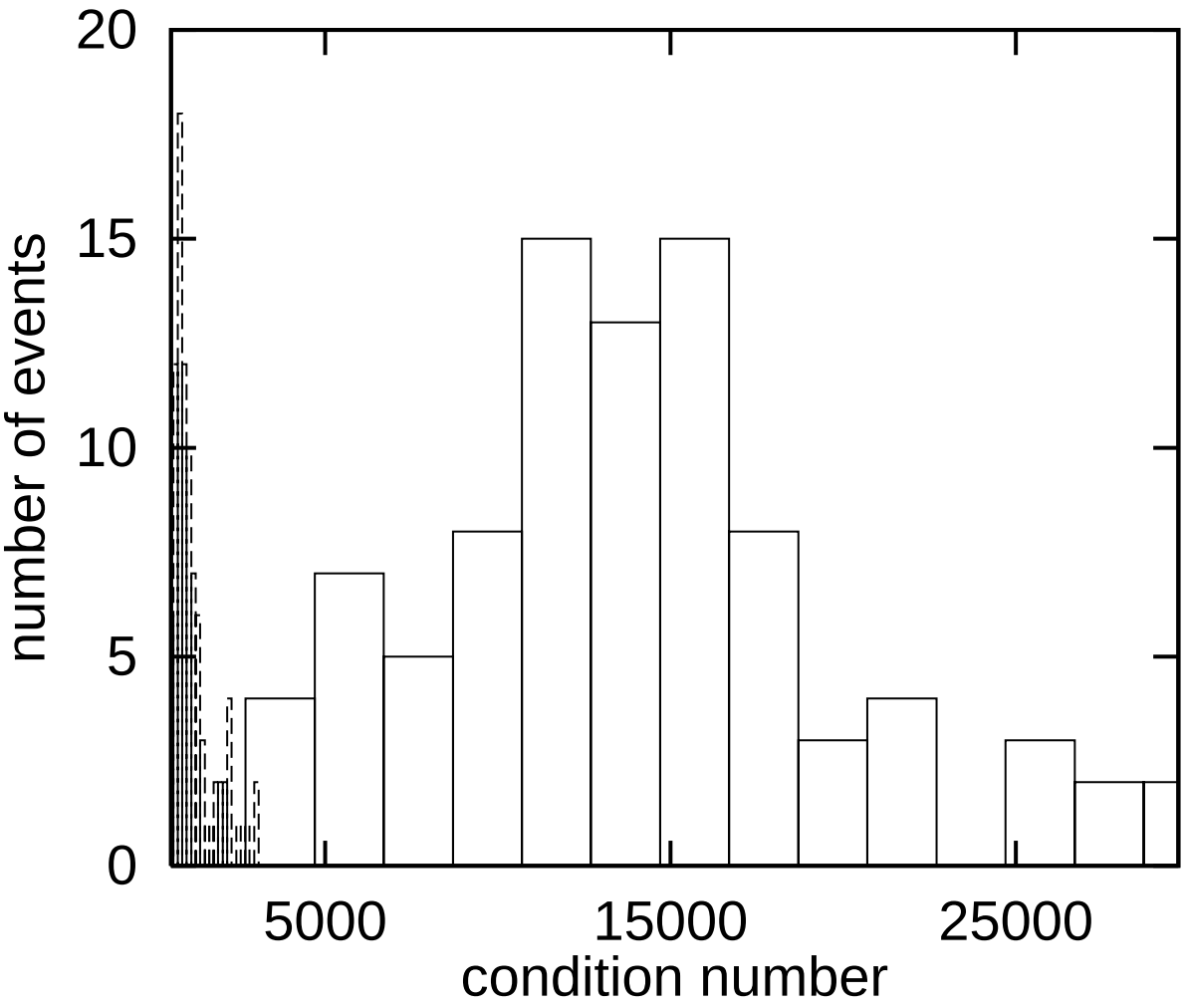
20
15
10
5
0
number of events
5000
15000
25000
condition number

Figure 3:

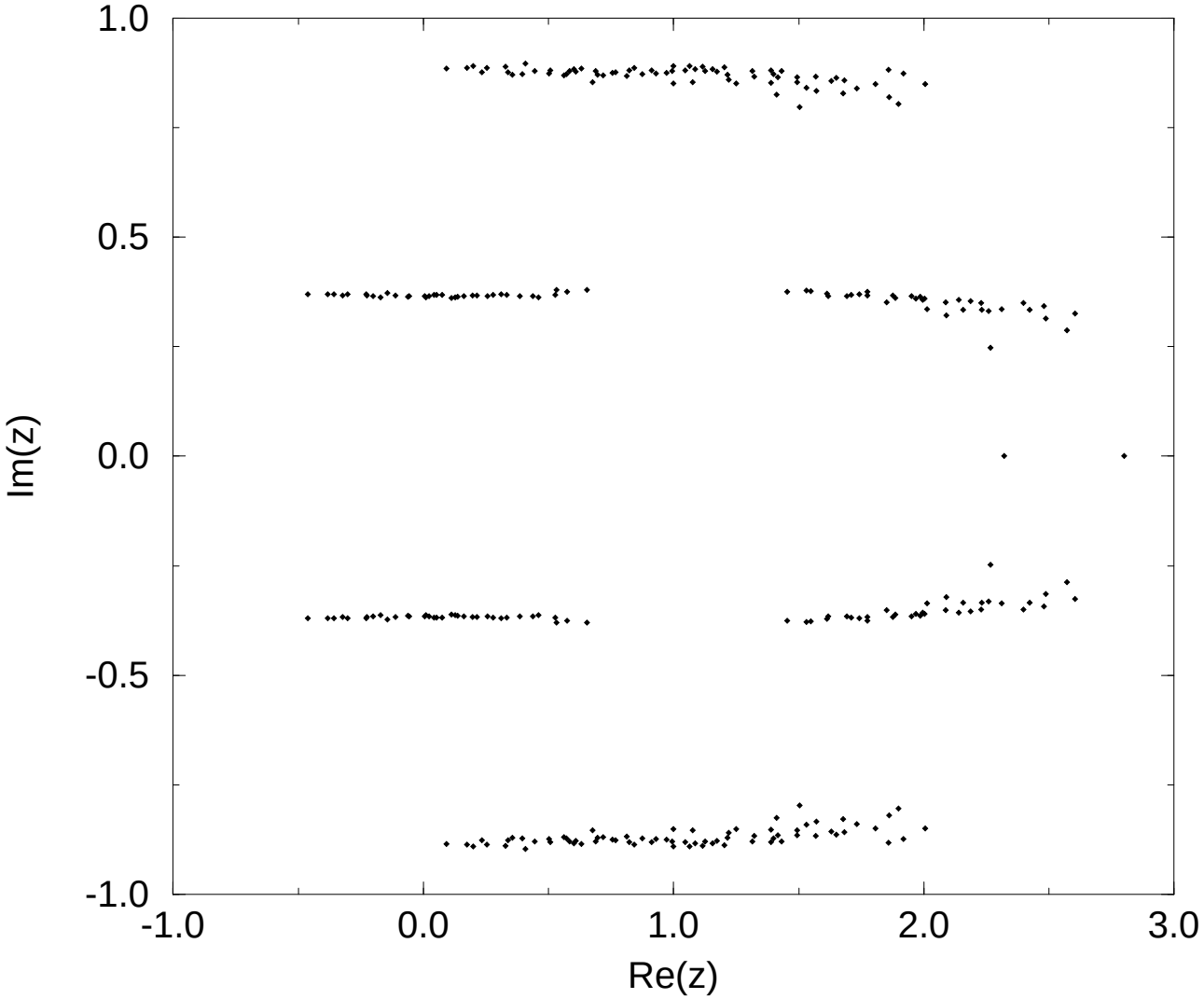

Figure 4:

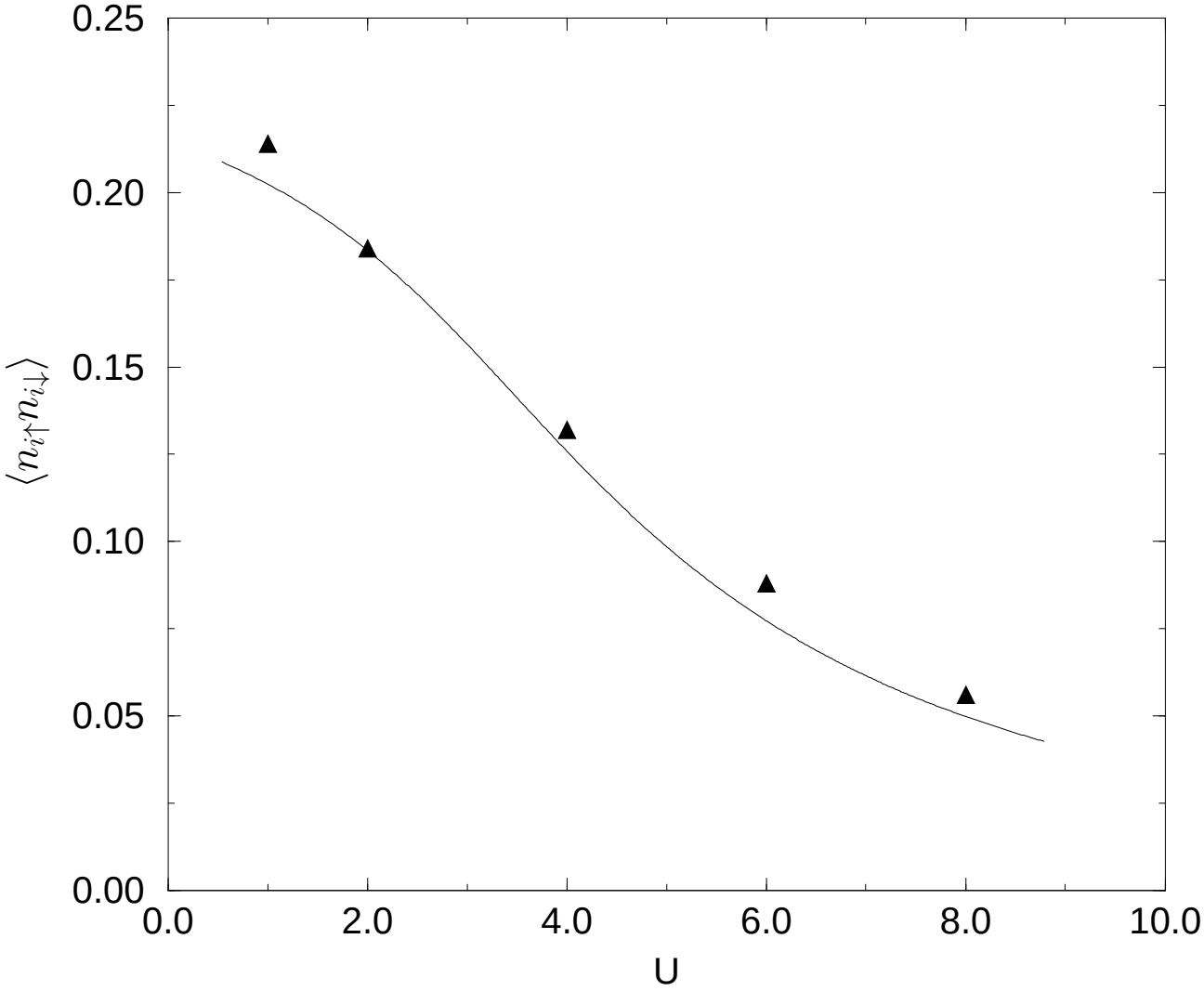
0.25
0.20
0.15
0.10
0.05
0.00
$\langle n_{i\uparrow} n_{i\downarrow} \rangle$
0.0
2.0
4.0
6.0
8.0
10.0
U

Figure 5:

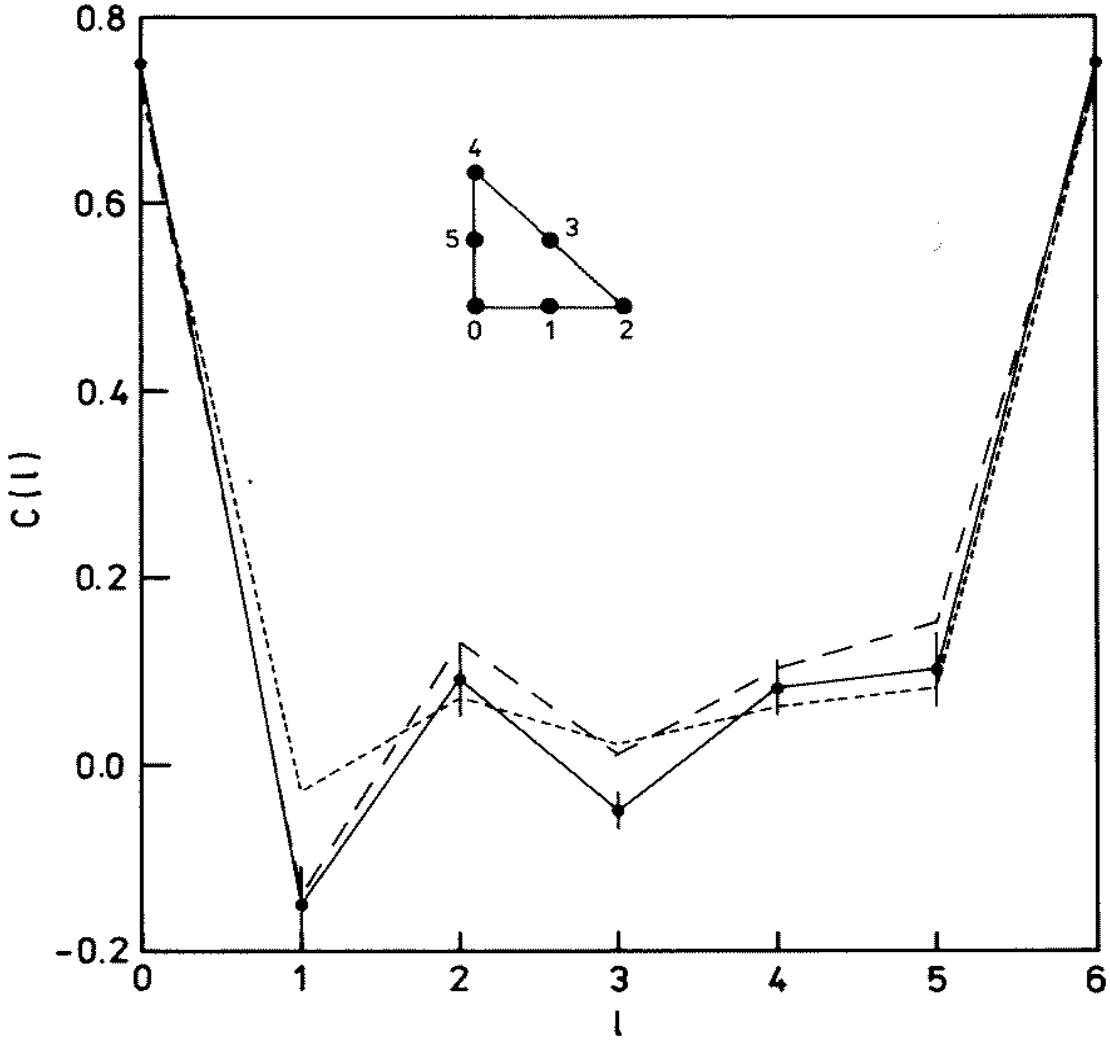

Figure 6:

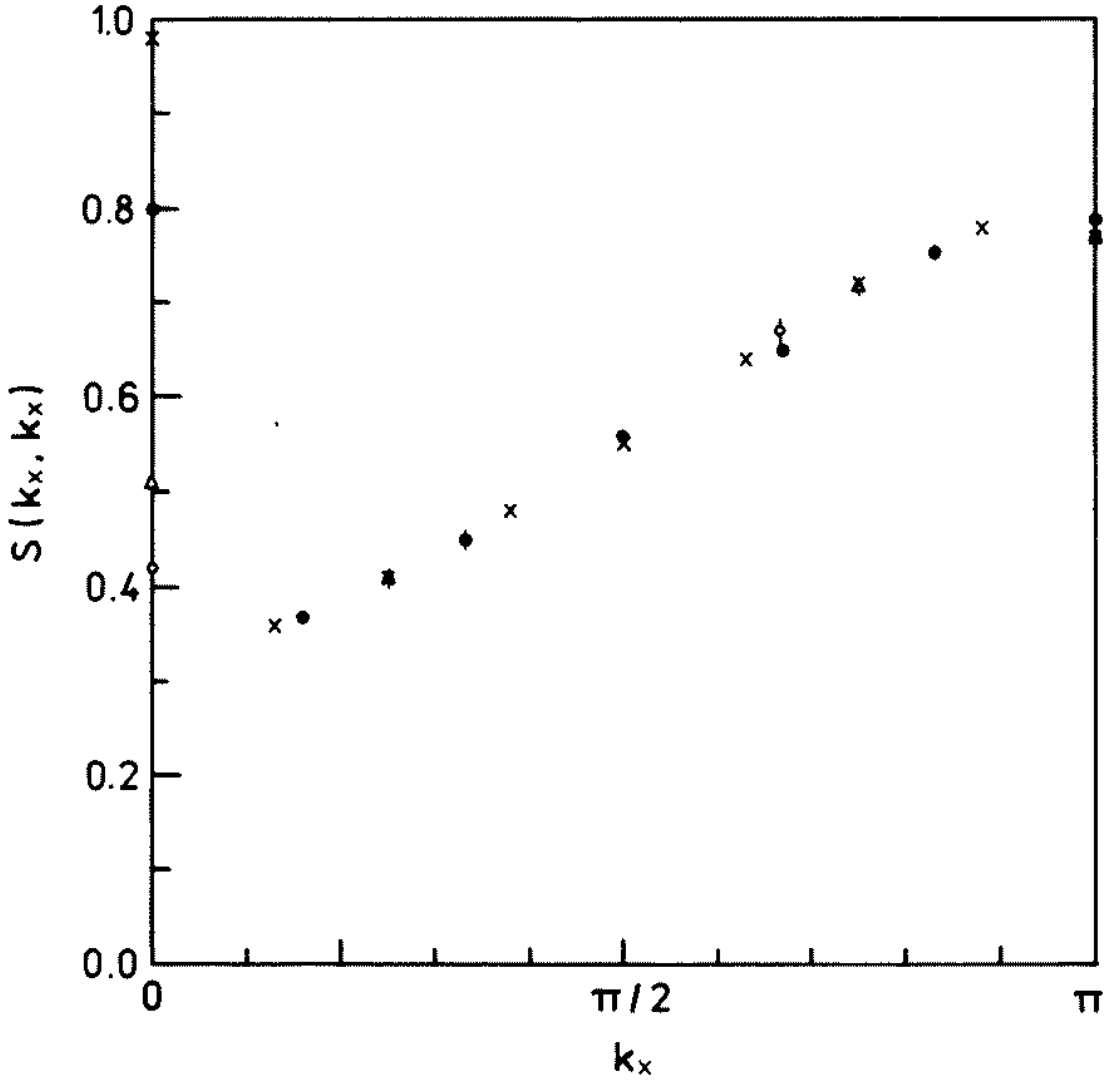

Figure 7:

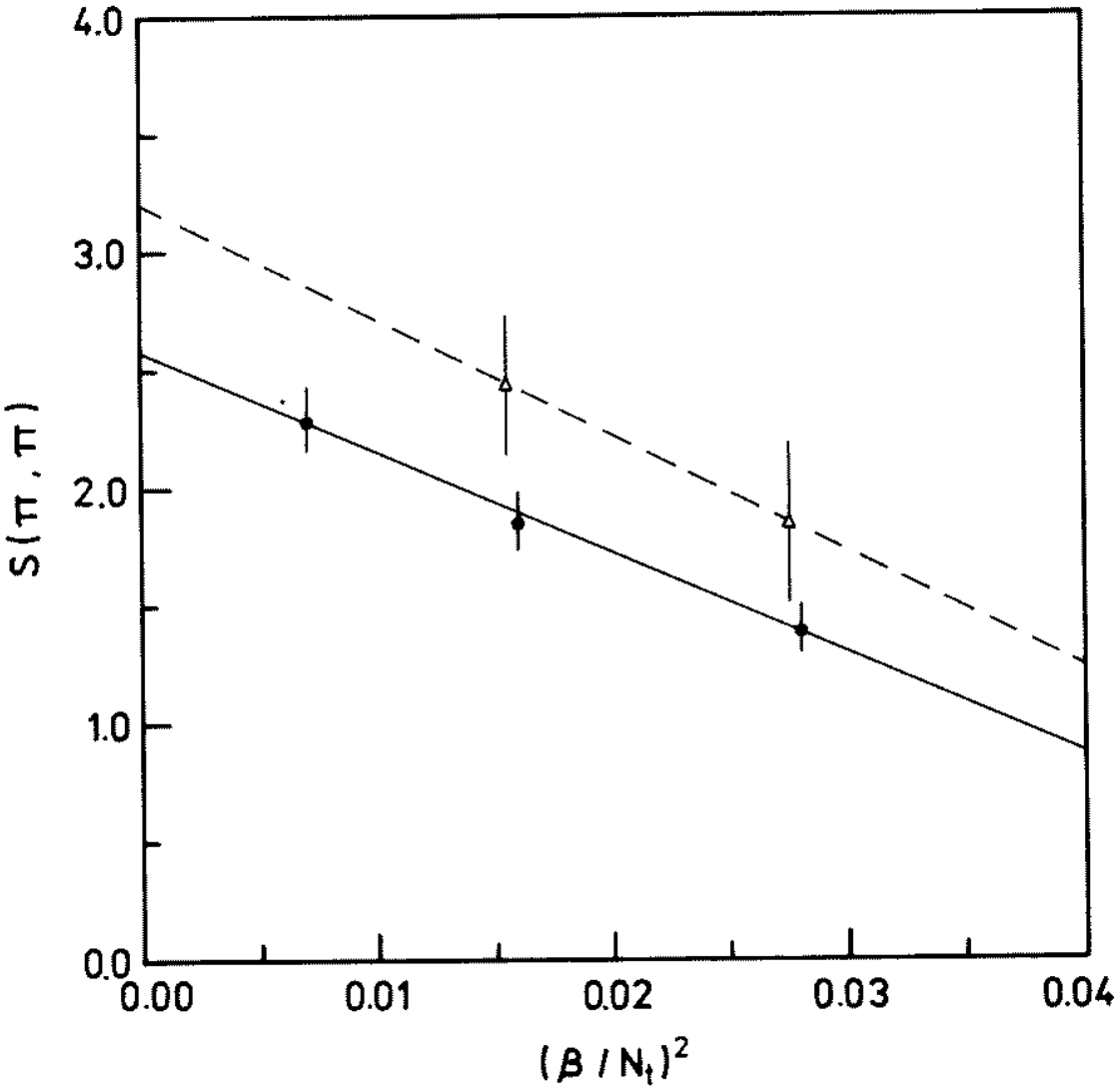

Figure 8:

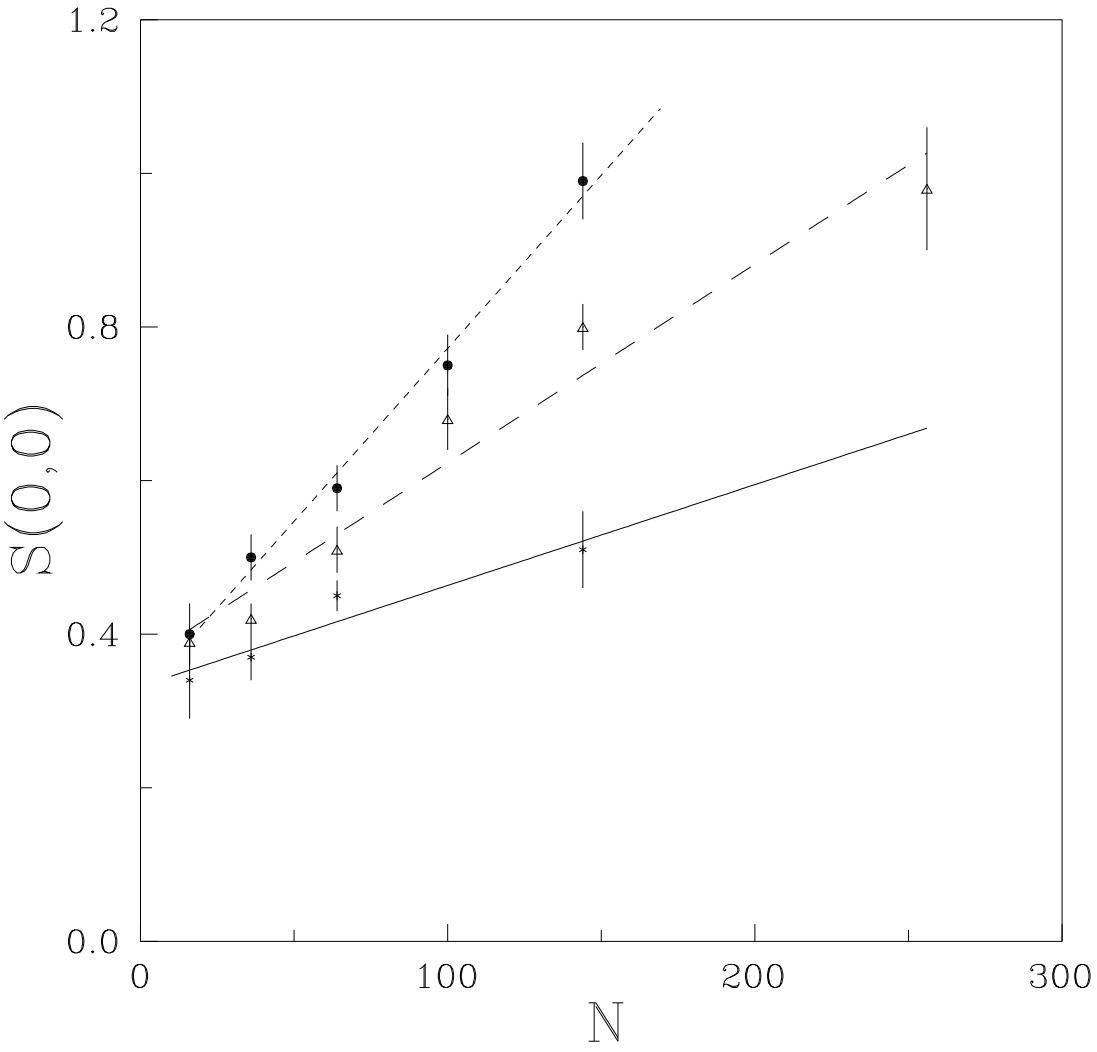

Figure 9:

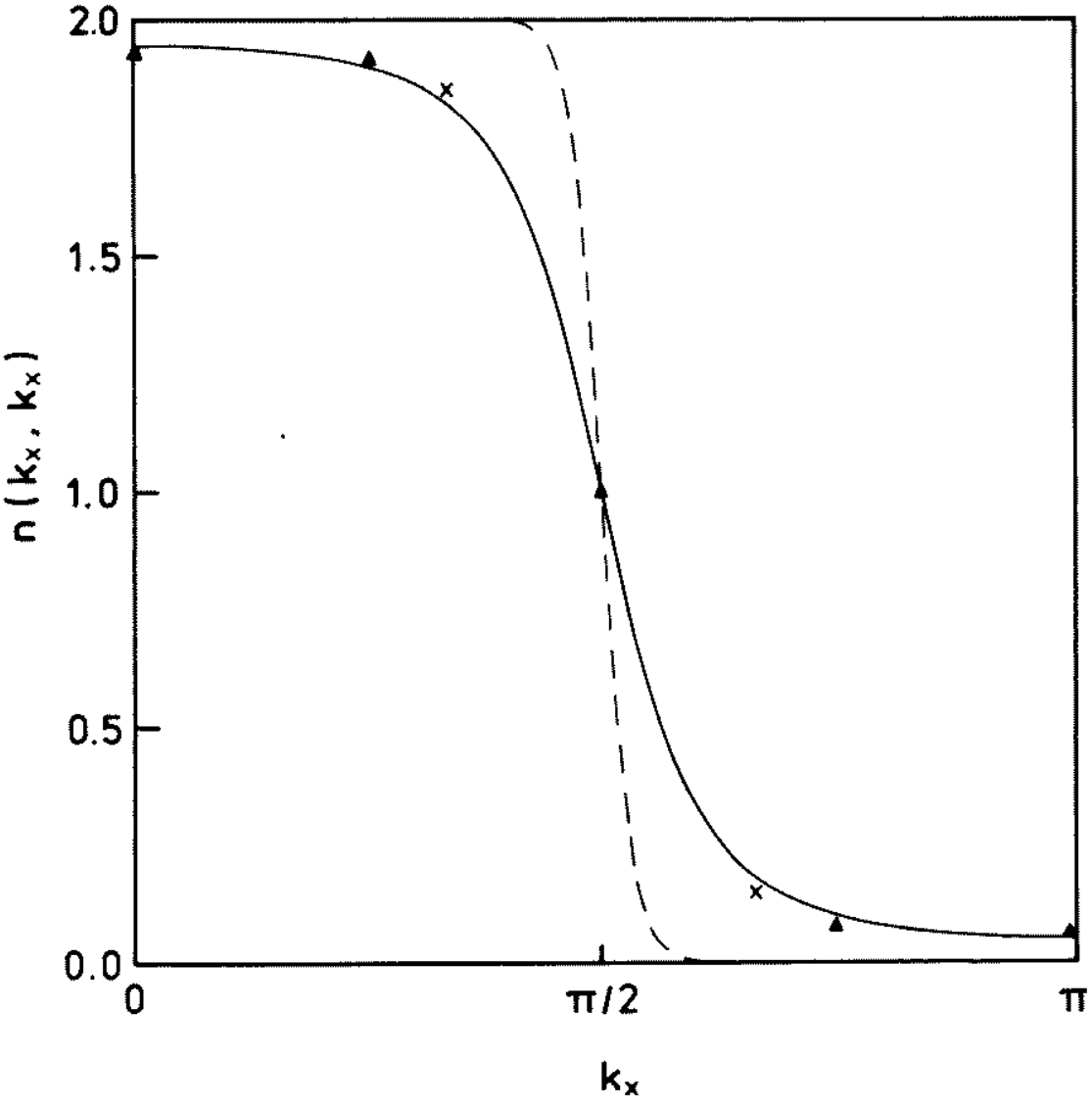

Figure 10:

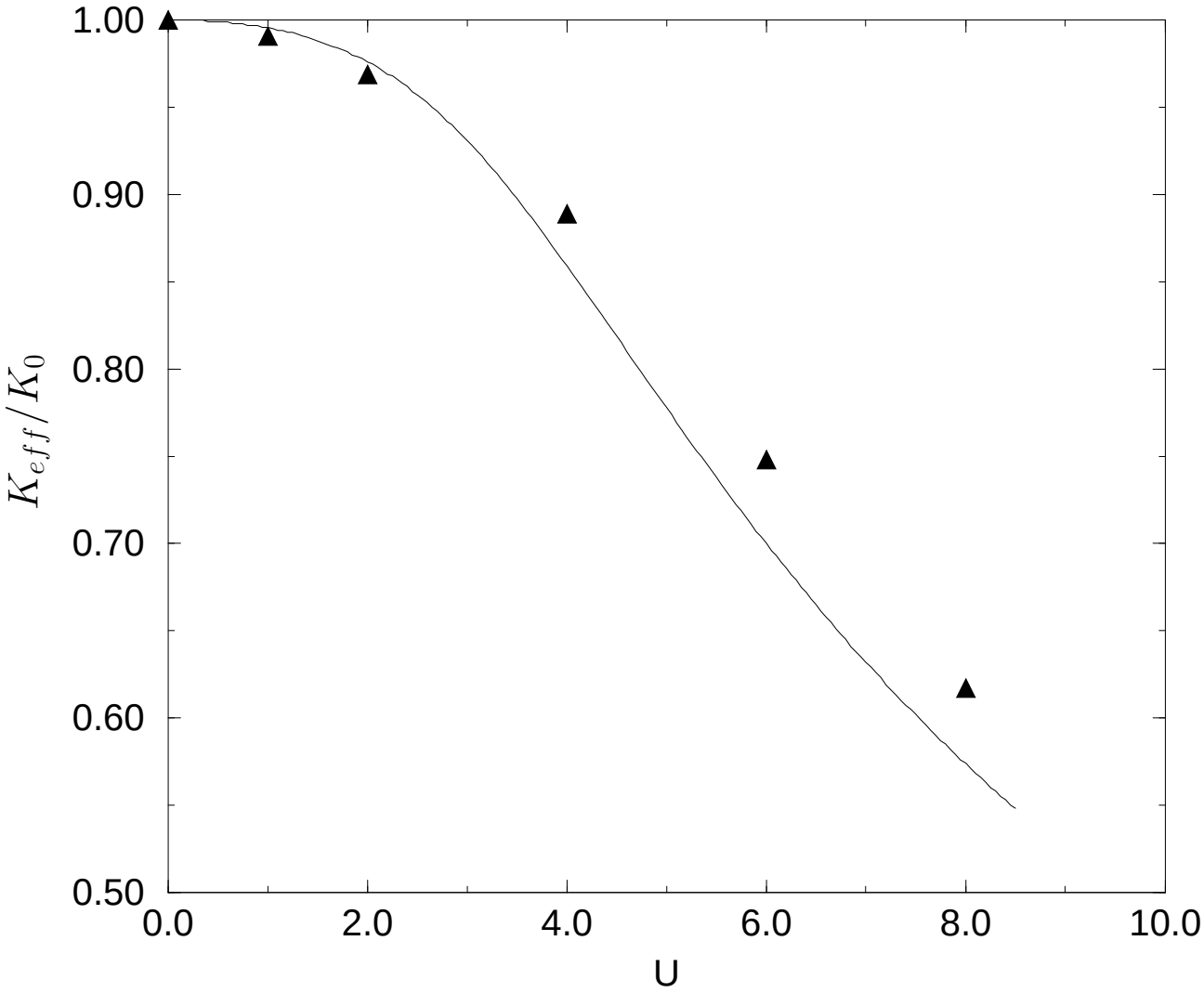

Figure 11: